Imidazo[2,1-b] [1,3,4]thiadiazoles with antiproliferative activity against primary and gemcitabine-resistant pancreatic cancer cells

Cascioferro, Stella; Petri, Giovanna Li; Parrino, Barbara; Carbone, Daniela; Funel, Niccola; Bergonzini, Cecilia; Mantini, Giulia; Dekker, Henk; Geerke, Daan; Peters, Godefridus J.; Cirrincione, Girolamo; Giovannetti, Elisa; Diana, Patrizia

published in
European Journal of Medicinal Chemistry
2020

DOI (link to publisher)
10.1016/j.ejmech.2020.112088

document version
Publisher's PDF, also known as Version of record

European Journal of Medicinal Chemistry 189 (2020) 112088

Contents lists available at ScienceDirect

European Journal of Medicinal Chemistry

journal homepage: http://www.elsevier.com/locate/ejmech

Research paper

Imidazo[2,1-*b*] [1,3,4]thiadiazoles with antiproliferative activity against primary and gemcitabine-resistant pancreatic cancer cells

Stella Cascioferro [a, 1], Giovanna Li Petri [a, b, 1], Barbara Parrino [a], Daniela Carbone [a], Niccola Funel [c], Cecilia Bergonzini [b], Giulia Mantini [b], Henk Dekker [b], Daan Geerke [d], Godefridus J. Peters [b], Girolamo Cirrincione [a], Elisa Giovannetti [b, e, **], Patrizia Diana [a, *]

[a] *Dipartimento di Scienze e Tecnologie Biologiche Chimiche e Farmaceutiche (STEBICEF), Università degli Studi di Palermo, Via Archirafi 32, 90123, Palermo, Italy*
[b] *Department of Medical Oncology, Amsterdam University Medical Center, VU University Cancer Center Amsterdam, De Boelelaan 1117, 1081HV, Amsterdam, the Netherlands*
[c] *Unit of Anatomic Pathology II, Azienda Ospedaliero-Universitaria Pisana, Via Roma 67, 56126, Pisa, Italy*
[d] *AIMMS Division of Molecular Toxicology, Department of Chemistry and Pharmaceutical Sciences, Faculty of Sciences, VU University Amsterdam, De Boelelaan 1108, 1081 HZ, Amsterdam, the Netherlands*
[e] *Fondazione Pisana per la Scienza, Via Ferruccio Giovannini 13, 56017, San Giuliano Terme, Pisa, Italy*

ARTICLE INFO

Article history:
Received 1 October 2019
Received in revised form
16 January 2020
Accepted 20 January 2020
Available online 25 January 2020

Keywords:
Imidazo[2,1-*b*][1,3,4]thiadiazole derivatives
Pancreatic ductal adenocarcinoma
Antiproliferative activity
Inhibition of migration
Spheroids shrinkage
Modulation of EMT
PTK2/FAK

ABSTRACT

A new series of eighteen imidazo [2,1-*b*] [1,3,4]thiadiazole derivatives was efficiently synthesized and screened for antiproliferative activity against the National Cancer Institute (NCI-60) cell lines panel. Two out of eighteen derivatives, compounds **12a** and **12h**, showed remarkably cytotoxic activity with the half maximal inhibitory concentration values (IC_{50}) ranging from 0.23 to 11.4 μM, and 0.29–12.2 μM, respectively. However, two additional compounds, **12b** and **13g**, displayed remarkable *in vitro* antiproliferative activity against pancreatic ductal adenocarcinoma (PDAC) cell lines, including immortalized (SUIT-2, Capan-1, Panc-1), primary (PDAC-3) and gemcitabine-resistant (Panc-1R), eliciting IC_{50} values ranging from micromolar to sub-micromolar level, associated with significant reduction of cell-migration and spheroid shrinkage. These remarkable results might be explained by modulation of key regulators of epithelial-to-mesenchymal transition (EMT), including E-cadherin and vimentin, and inhibition of metalloproteinase-2/-9. High-throughput arrays revealed a significant inhibition of the phosphorylation of 45 tyrosine kinases substrates, whose visualization on Cytoscape highlighted PTK2/FAK as an important hub. Inhibition of phosphorylation of PTK2/FAK was validated as one of the possible mechanisms of action, using a specific ELISA. In conclusion, novel imidazothiadiazoles show potent antiproliferative activity, mediated by modulation of EMT and PTK2/FAK.

1. Introduction

The synthesis of hybrid molecules, bearing two or more different biologically active scaffolds in a single structure, is regarded as one of the most valuable approaches in drug development in order to obtain new therapeutic strategies to treat oncological diseases [1–3].

The design of anticancer drugs characterized by two moieties with antitumor activity led to the development of a number of molecules with improved biological potential compared to the parent compounds. In particular, hybrid anticancer drugs showed improved specificity, a greater ability to overcome drug-resistance mechanisms, better patient compliance and lower side effects [4,5].

The simultaneous presence of two pharmacophores often led to a synergism of the biological activities and therefore to the capability to act towards more than one target. Many examples of hybrid compounds with promising cytotoxic properties have been

* Corresponding author. Dipartimento di Scienze e Tecnologie Biologiche Chimiche e Farmaceutiche (STEBICEF), Università degli Studi di Palermo, Via Archirafi 32, 90123, Palermo, Italy
** Corresponding author. Department of Medical Oncology, Amsterdam University Medical Center, VU University Cancer Center Amsterdam, De Boelelaan 1117, 1081HV, Amsterdam, the Netherlands.
E-mail addresses: e.giovannetti@amsterdamumc.nl (E. Giovannetti), patrizia.diana@unipa.it (P. Diana).
[1] Equally contributed.

https://doi.org/10.1016/j.ejmech.2020.112088
0223-5234/

reported in the latest years. Singla and collaborators described remarkable antiproliferative activity against the NCI-60 cell lines panel of benzimidazole-triazine hybrids **1** (Fig. 1) which showed IC_{50} values from the low micromolar to the nanomolar range [6]. The pyrimidine-triazole hybrids **2** (Fig. 1) exhibited potent anticancer activity against the B16–F10 murine melanoma cancer cell line due to their ability in reducing the pro-caspase 3 level while increasing the p53 and active-caspase 3 levels [7]. Pyrazole-benzofuran hybrids **3** (Fig. 1) emerged as promising anticancer compounds against human pancreatic (Panc-1 and PaCa-2 cells), lung (A549 and H-460), breast (MCF-7), colon (HT-29) and prostate (PC-3) cancer, with IC_{50} values in the range of 0.9–2.2 μM (Fig. 1) [8].

The imidazo [2,1-*b*] [1,3,4]thiadiazole nucleus has been considered a privileged scaffold for the development of molecules with various pharmacological activities, such as anticancer [9], analgesic [10], anti-leishmanial [11], antioxidant [12], antitubercular [13], anticonvulsant [14], and antibacterial [15,16].

Concerning the antitumor activity, many imidazo [2,1-*b*] [1,3,4] thiadiazole derivatives have been described as potent anticancer molecules acting on several targets against different tumor models. Compound **4** (Fig. 2) showed potent inhibitory activity (IC_{50} = 1.2 nM) against the activin receptor-like kinase 5 (ALK5) proving to be selective toward the P38α kinase [17]. The imidazo [2,1-*b*] [1,3,4]thiadiazole-5-carbaldehyde **5** (Fig. 2) was three fold more potent than melphalan, used as reference drug, against murine (L1210) and human (CEM) leukemia cells as well as against immortalized cervical cancer (HeLa) cells, eliciting IC_{50} values of 0.89 μM, 0.75 μM and 0.90 μM, respectively [18].

In the last decade the indole ring has emerged among the scaffolds recognized as privileged pharmacophores for the development of new antitumor compounds [19–26].

The indole derivative **6** was described for its potent antiproliferative activity against diffuse malignant peritoneal mesothelioma (DMPM) cell. Nortopsentin analogue **6** potently inhibited CDK1 activity eliciting an IC_{50} value of 0.86 μM and consequently induced a marked cell cycle arrest at the G2/M phase, which was paralleled by an increase in the apoptotic rate [27].

Therefore, on the basis of the interesting anticancer properties described for imidazo [2,1-*b*] [1,3,4]thiadiazole and indole scaffolds, we decided to evaluate the cytotoxic activity of a library of thirty-six 3-(6-phenylimidazo [2,1-*b*] [1,3,4]thiadiazol-2-yl)-1*H*-indole derivatives. In particular derivative **7** (Fig. 3) was effective against all the tested cancer cell lines showing GI_{50} values ranging from 1.02 to 9.21 μM [28].

These preliminary results prompted further studies on nitrogen heterocyclic systems endowed with antitumor activity [29–35] and we synthesized eighteen new 3-(imidazo [2,1-*b*] [1,3,4]thiadiazol-2-yl)-1*H* indole analogues in order to evaluate how structural modifications on the indole nucleus, introduction of an aldehyde group at the position 5 of the imidazothiadiazole scaffold or the replacement of the phenyl ring at the position 6 with a thiophene ring could influence the anticancer activity of this class of compounds.

We decided to test our new compounds on clinically-relevant models of pancreatic ductal adenocarcinoma (PDAC). This tumor is an extremely aggressive neoplasm, predicted to become the second leading cause of cancer-related deaths before 2030 [36]. Cytotoxic chemotherapy remains the mainstay of treatment for most PDAC patients. Treatment with 5-fluorouracil, leucovorin, irinotecan and oxaliplatin (FOLFIRINOX) or with a combination of gemcitabine and nab-paclitaxel, represent the standard-of-care for unresectable patients, and recent data support the use of FOLFIRINOX as adjuvant therapy after surgical resection [37]. However, PDAC is broadly chemoresistant, with a 5-year survival rate below 9%, and novel, more effective therapeutics for PDAC remain an important unmet need [38–40].

2. Chemistry

The new imidazothiadiazole derivatives **12**–**14** were efficiently synthesized following the synthetic route described in Scheme 1.

The commercially available indole-3-carbonitrile **9a** and the derivatives **9b-e**, prepared by reaction of the appropriate 1*H*-indole

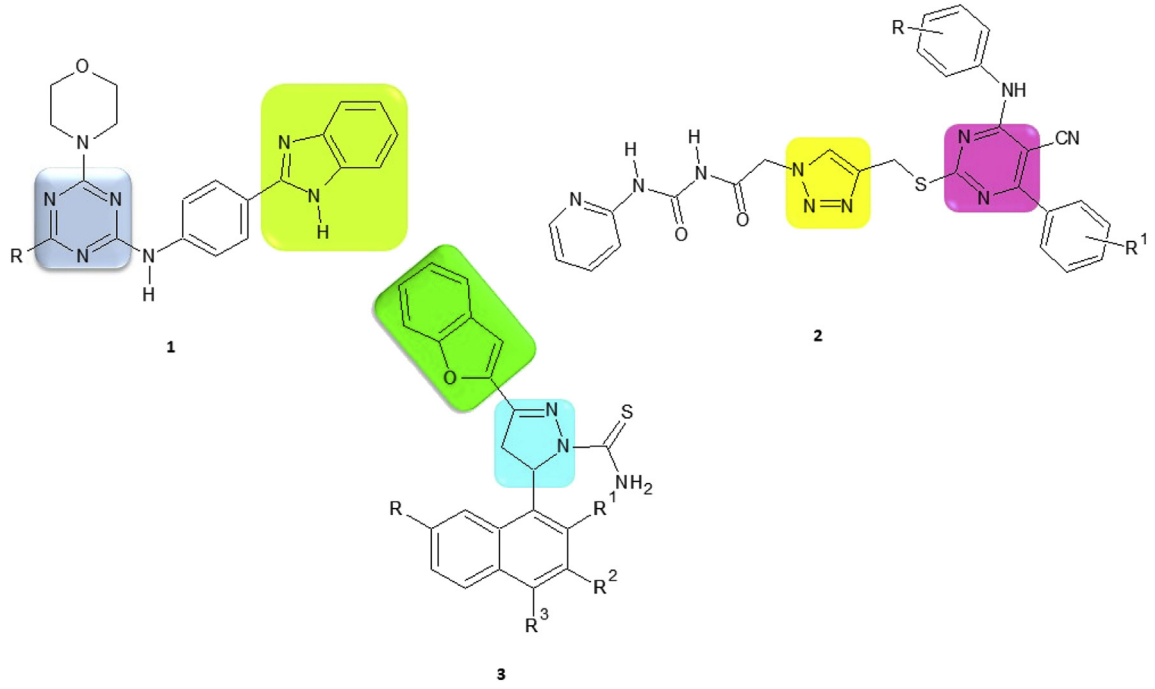

Fig. 1. Chemical structures of benzimidazole-triazine hybrids **1**, pyrimidine-triazole hybrids **2**, pyrazole-benzofuran hybrids **3**.

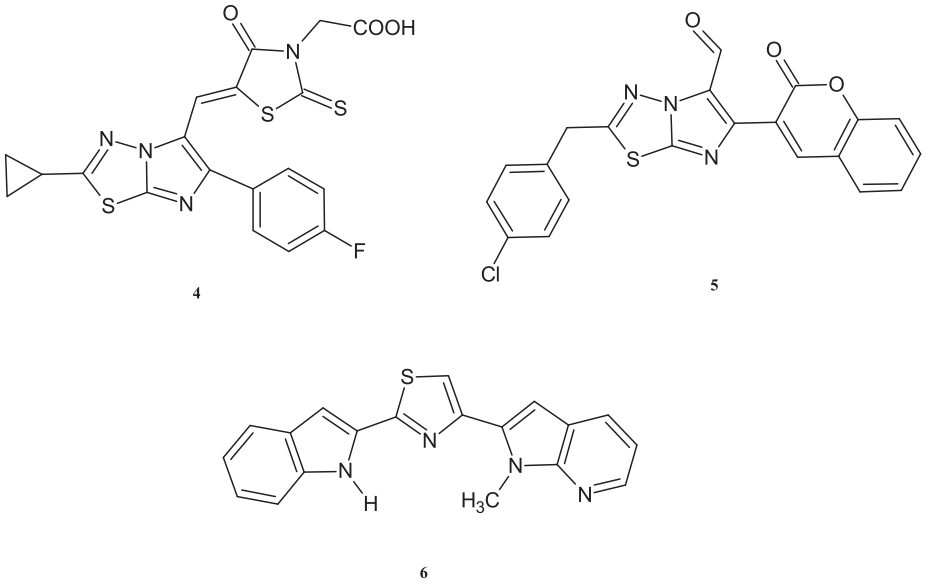

Fig. 2. Chemical structures of the anticancer compounds **4**–**6**.

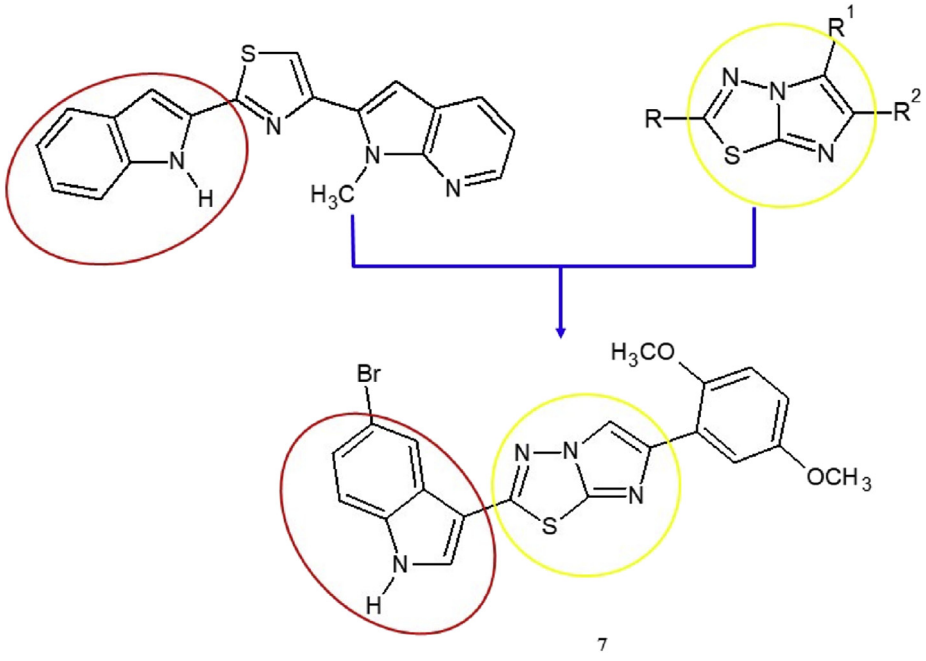

Fig. 3. Hybrid compound **7** obtained by combining the two bioactive scaffolds indole and imidazothiadiazole.

with chlorosulfonyl isocyanate (CSI), were subjected to a methylation for obtaining the corresponding 1-methyl-1*H*-indole-3-carbonitriles **10a-e** [16]. The 5-(1*H*-indol-3-yl)-1,3,4-thiadiazol-2-amines **11a-j** were obtained in excellent yields (92–100%) by treating the proper derivatives **9a-e** or **10a-e** with thiosemicarbazide.

The 1,3,4-thiadiazol-2-amines **11a-j** underwent a reaction with the appropriate α-bromoacetyl compounds in refluxing ethanol to give the hydrobromide derivatives **12a-r**. Some of such hydrobromides, **12a**,**b**,**d**,**e**,**f**,**h**, were isolated as pure compounds (yields 55–68%) and were characterized without further purifications. Instead, hydrobromides **12c**,**g**,**i**,**j** were treated with saturated aqueous $NaHCO_3$ solution producing the corresponding free bases **13** which were purified by column chromatography providing specimens with suitable analytical and spectral data (yields 58–80%).

Finally, the free bases **13k-r,** prepared through the treatment of the corresponding hydrobromides **12** with saturated aqueous $NaHCO_3$ solution, were subjected to a reaction of formylation using standard Vilsmeier conditions to give the imidazo [2,1-*b*] [1,3,4] thiadiazole derivatives **14k-r** (yields 70–90%) (Table 1).

Data on physicochemical properties of the compounds are reported in the Supplementary results and Supplementary Tables 1–2.

Reagents and conditions: i) CH_3CN, CSI, 0 °C, 2 h, then DMF, 0 °C, 1.5 h (98–100%); ii) DMF, $(CH_3O)_2CO$, K_2CO_3, 130 °C, 3.5 h (98–100%); iii) trifluoroacetic acid, thiosemicarbazide, 60 °C, 3.5 h

Table 1
New 3-(imidazo [2,1-*b*] [1,3,4]thiadiazol-2-yl)-1*H*-indole derivatives **12**–**14.**

Comp	R	R^1	R^2	Yield
12a	H	H	tiophen-3-yl	57%
12b	H	CH_3	tiophen-3-yl	55%
12d	Br	CH_3	tiophen-3-yl	68%
12e	Cl	H	tiophen-3-yl	63%
12f	Cl	CH_3	tiophen-3-yl	68%
12h	F	CH_3	tiophen-3-yl	58%
13c	Br	H	tiophen-3-yl	58%
13g	F	H	tiophen-3-yl	80%
13i	OCH_3	H	tiophen-3-yl	58%
13j	OCH_3	CH_3	tiophen-3-yl	70%
14k	H	H	C_6H_5	71%
14l	H	CH_3	C_6H_5	91%
14m	H	H	4-F-C_6H_4	81%
14n	H	H	3OCH_3–C_6H_4	60%
14o	H	H	2,5-OCH_3-C_6H_3	82%
14p	H	CH_3	2,5-OCH_3-C_6H_3	70%
14q	H	H	4-NO_2-C_6H_4	75%
14r	Br	H	2,5-OCH_3-C_6H_3	90%

(98–100%); iv) anhydrous ethanol, reflux, 24 h (42–80%); v) $NaHCO_3$ saturated aqueous solution (58–80%); vi) $POCl_3$, DMF, 0–5 °C, then compound **13**, DMF, 70 °C, 5 h.

3. Results and discussion

3.1. Antiproliferative activity

The newly synthesized imidazo [2,1-*b*] [1,3,4]thiadiazoles **12a,b,d,e,f,h, 13c,g,i,j** and **14k,l,n,o,p** were submitted to the National Cancer Institute (NCI; Bethesda, MD) for the pharmacological evaluation of their antitumor activity. They were initially pre-screened according to the NCI protocol at one-dose of 10 μM on the full panel of 60 human cancer cell lines derived from 9 cancer cell types and grouped into disease subpanels including leukemia, non-small cell lung, colon, central nervous system, melanoma, ovarian, renal, prostate, and breast cancers. The **12a** and **12h** derivatives were selected for further screening at five concentrations at 10-fold dilution (10^{-4}-10^{-8} M) on the full panel. As shown in Table 2, both derivatives have interesting *in vitro* anticancer activity with GI_{50} values ranging from micromolar to sub-micromolar level, i.e., 0.23–11.4 μM, and 0.29–12.2 μM, respectively (Table 2).

In order to expand the NCI panel, we evaluated the *in vitro* antiproliferative activity of the compounds **12a,b,d,e,f,h**, **13c,g,i,j** and **14k-r** on a panel of PDAC cells, including SUIT-2, Capan-1 and Panc-1, by Sulforhodamine-B (SRB) assay. PDAC is indeed broadly chemoresistant tumor, with a 5-year survival rate below 9%, and novel, more effective therapeutics for PDAC remain an important unmet need.

A pre-screening assay was initially performed at concentrations of 0.1, 1 and 16 μM. We then expanded the cytotoxicity test, using at least 8 different concentrations (from 125 nM to 16 μM) on the most promising compounds, in order to define more accurate half-maximal inhibitory concentration (IC_{50}) values. The compounds **12a**,**b**,**h** and **13g** exhibited remarkable antiproliferative activity on all the preclinical models with IC_{50} values in the range from 0.85 to 4.86 μM (Table 3).

PDAC is notoriously resistant to chemotherapy or radiotherapy. For several decades, gemcitabine monotherapy has been used as a first-line treatment for metastatic PDAC and is still a cornerstone of PDAC treatment in all stages of this disease. However, this drug has limited clinical effects caused by primary PDAC resistance, as well as by the development of resistance within a few weeks from treatment initiation [41]. Therefore, new therapeutic agents should be tested for their ability to circumvent gemcitabine chemoresistance. For this reason, we assessed the cytotoxic activity of the compounds **12a**,**b**,**h** and **13g** in the Panc-1R cells, a gemcitabine-resistant sub-clone obtained by continuous incubation of Panc-1 with 1 μM of the drug [41]. Notably, all these compounds showed antiproliferative activity against Panc-1R, with IC50 ranging from 2.2 ± 0.37 μM (compound **12b**) to 3.9 ± 0.25 μM (compound **13g)** as reported in Fig. 4.

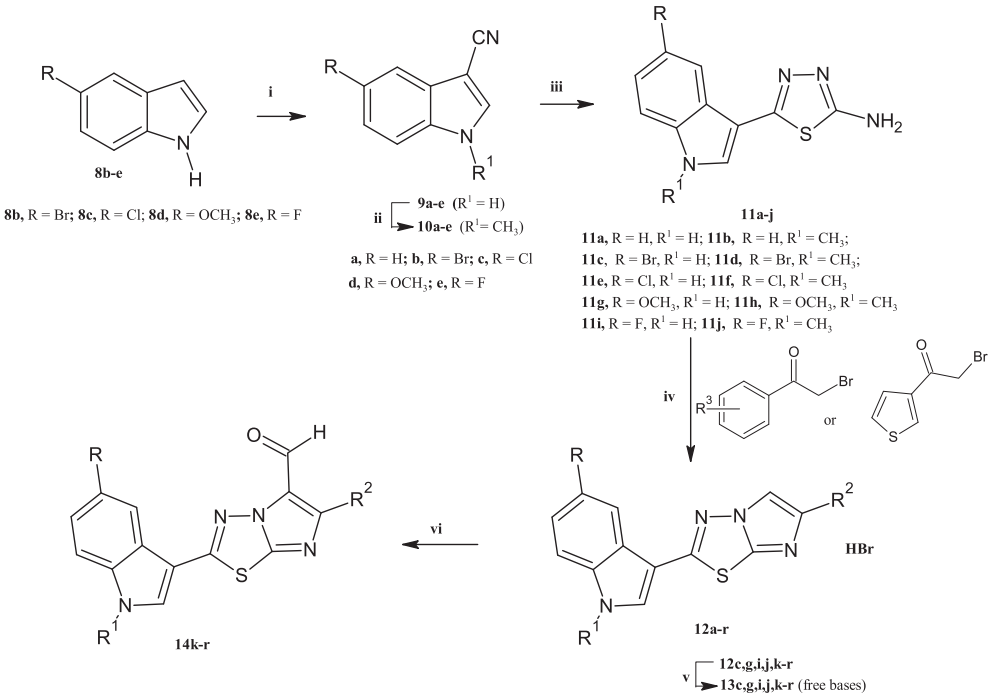

Scheme 1. Synthesis of 3-(imidazo [2,1-*b*] [1,3,4]thiadiazol-2-yl)-1*H*-indole derivatives **12**–**14.**

Table 2
GI_{50} and TGI of the compounds **12a** and **12h**.[a]

Panel/Cell line	12a		12h	
	GI_{50} (μM)	TGI (μM)	GI_{50} (μM)	TGI (μM)
Leukemia				
CCRF-CEM	2.19	27.2	2.54	>100
HL-60 (TB)	0.76	20.9	1.34	15.5
K-562	0.38	39.9	0.45	>100
RPMI-8226	1.47	15.4	3.01	27
Non-Small Cell Lung Cancer				
A549/ATCC	1.72	>100	2.85	99.5
EKVX	1.99	>100	2.51	>100
HOP-62	1.58	39.9	1.92	23.1
HOP-92	5.46	>100	12.2	76.9
NCI−H226	9.94	>100	4.56	35.8
NCI−H23	4.47	>100	3.82	>100
NCI−H322 M	4.85	52.7	4.71	>100
NCI−H460	0.57	>100	1.73	17.1
NCI−H522	0.75	>100	1.62	24.5
Colon Cancer				
HCC-2998	2.99	26.7	5.64	33.9
HCT-116	0.63	70.6	2.04	26.4
HCT-15	0.49	15.6	0.61	>100
HT29	0.41	10.2	0.48	14.8
KM12	0.50	10.5	1.04	>100
SW-620	0.43	>100	0.48	>100
CNS Cancer				
SF-268	3.84	>100	6.58	>100
SF-295	1.74	6.44	2.24	9.39
SF-539	1.49	4.60	2.18	7.54
SNB-19	2.56	>100	3.44	>100
SNB-75	0.45	8.09	1.29	6.45
U251	1.21	17	2.76	17.9
Melanoma				
MALME-3M	10.4	36.9	1.81	31.6
M14	0.75	15.8	1.05	>100
MDA-MB-435	0.23	0.68	0.29	1.13
SK-MEL-2	1.08	23.8	1.59	7.29
SK-MEL-28	4.74	44.0	7.23	>100
SK-MEL-5	0.71	15.1	1.80	12.9
UACC-257	11.4	98.3	7.90	>100
UACC-62	0.74	18.7	1.93	>100
Ovarian Cancer				
IGROV1	1.79	>100	1.93	>100
OVCAR-3	0.92	9.02	2.06	9.67
OVCAR-4	4.42	>100	5.77	>100
OVCAR-5	4.27	76.4	8.24	84.4
OVCAR-8	2.72	>100	4.53	>100
NCI/ADR-RES	0.56	>100	0.99	19.1
SK-OV-3	2.80	82.7	3.47	70.9
Renal Cancer				
786−0	3.06	>100	7.62	52.3
A498	5.97	23.6	4.09	50.0
ACHN	3.23	52.5	3.39	86.8
CAKI-1	1.00	>100	2.42	57.4
RXF 393	2.05	50.0	1.59	5.73
SN12C	1.15	>100	4.71	>100
TK-10	5.21	33.5	4.92	19.4
UO-31	1.71	>100	1.72	>100
Prostate Cancer				
PC-3	2.07	>100	3.19	>100
DU-145	2.86	>100	3.67	31.6
Breast Cancer				
MCF7	1.17	20.2	0.83	30.0
MDA-MB-231/ATCC	1.08	7.88	3.23	30.6
HS 578T	2.65	>100	2.34	13.4
BT-549	2.87	31.7	5.54	77.4
MDA-MB-468	2.92	27.8	1.44	5.47

[a] Data obtained from the NCI *in vitro* disease-oriented human tumor cell line screen. [b] GI_{50}: concentration that inhibit 50% net cell growth. [c] TGI total growth inhibition.

Our previous studies showed different genetic and epigenetic modifications, including splicing and phosphoproteomics aberrations [42,43], underlying the molecular mechanisms of gemcitabine-resistance, and further studies will be carried out to identify how our new compounds counteract these mechanisms. Moreover, the compounds **12a**,**b**,**h** and **13g** were tested on a primary patient-derived PDAC cell culture, PDAC-3 (Fig. 4B and C). This cellular model was chosen since our previous studies showed that its genetic and histological features were similar to the original tumor [44]. In order to maintain the original characteristics of the primary tumor, particularly from the genetic point of view, these cells have been kept in culture only for a few passages. As shown in Fig. 4B the new imidazothiadiazoles maintained their antiproliferative activity on PDAC-3 cells, with IC_{50} values slightly higher in comparison to the values reported on the previously mentioned cancer cell lines. The phase contrast microscopy images in Fig. 4C highlighted the antiproliferative activity of compounds **12a** and **12b** (central and right panel, respectively) compared to untreated cells (left picture) after 72 h of the treatment.

Because of their remarkable antiproliferative activity the compounds **12a**,**b**,**h** and **13g** were selected for following mechanistic studies, in order to unravel the mechanisms underlying their anticancer activity.

Despite compound **7** has shown interesting GI_{50} values against all the tested cancer cell lines in the NCI screening, preliminary biological evaluations of analogues **13k,l,n,p,r** showed limited antiproliferative activity [28]. We evaluated the citotoxicity of the compounds **13m, 13o** and **13q** on SUIT-2, Capan-1 and Panc-1 but the IC_{50} values were above 16 μM.

Finally, we performed additional experiments to evaluate the *in vitro* cytotoxicity of the new compounds **12a** and **12b** against the normal fibroblasts Hs27. The results of these experiments allowed us to calculate the selectivity index (SI, IC_{50} non-tumor cell line/IC_{50} tumor cell line), which was 4.5 and 7.2 for compounds 12a and 12b, respectively, and therefore our compounds have SI similar to Gemcitabine and 5-fluorouracil and were regarded as highly cancer selective compared to the primary pancreatic cells PDAC3 (Supplementary Table 3).

3.2. Volume reduction of PDAC-3-derived tumor spheres

Two-dimensional cytotoxicity assay obviously provide a useful method to screen libraries of compounds with high-throughput efficiency, but they are not capable of resembling the complex architecture and biology of solid tumors, which grow in three-dimensions (3D) [45]. For this reason we evaluated two of our most promising compounds (emerging from monolayer assay) on 3D spheroids of PDAC-3 cells. These primary cultures are indeed able to form spheroids that are more representative of the aggregation of tumor cells in vivo, as also reported in our previous studies [46].

We treated spheroids with compounds **12a** and **12b** after 3 days of growth, at 5-times the IC_{50}, and we took a picture which represent the Day 1. Then the treatment was repeated every four days (Day 5 and Day 8) and pictures were taken immediately before that (Fig. 5A).

Reduction of the size of spheroids was calculated by measuring their area with ImageJ. As shown in Fig. 5B, after five, but considerably more after eight days, both compounds clearly showed their ability to hinder the spheroids formation. This reduction is shown as the fold-change between treated spheroids compared to the controls and was statistically significant (p-value < 0.0001). Therefore, these two compounds retained their activity in a 3D model.

Table 3
Antiproliferative activity of compounds **12a,b,d,e,f,h**, **13c,g,i,j** and **14k-r** on SUIT-2, Capan-1 and Panc-1 cell lines.

IC_{50}[a] (μM) ± SEM[b]			
Cell lines			
Comp	SUIT-2	Capan-1	Panc-1
12a	**0.85 ± 0.018**	**1.19 ± 0.06**	**1.70 ± 0.20**
12b	**0.99 ± 0.078**	**1.35 ± 0.04**	**1.69 ± 0.10**
12d	>16	>16	>16
12e	>16	>16	>16
12f	>16	>16	>16
12h	**1.78 ± 0.017**	**1.93 ± 0.25**	**2.37 ± 0.028**
13c	>16	>16	>16
13g	**2.16 ± 0.039**	**4.52 ± 0.48**	**4.86 ± 0.5**
13i	>16	>16	>16
13j	>16	>16	>16
14k	9.56 ± 0.34	10.5 ± 0.21	12.41 ± 0.16
14l	>16	>16	>16
14m	7.93 ± 0.23	8.83 ± 0.17	10.53 ± 037
14n	11.49 ± 0.36	>16	>16
14o	13 ± 1.13	>16	>16
14p	12.49 ± 0.18	5.73 ± 0.086	>16
14q	5.32 ± 0.29	6.1 ± 0.019	3.61 ± 0.4
14r	8.7 ± 0.20	8.24 ± 0.08	10.56 ± 0.11
gemcitabine	0.01 ± 0.001	0.02 ± 0.001	0.15 ± 0.01
5-fluorouracil	0.91 ± 0.15	0.47 ± 0.13	4.3 ± 0.42

[a] The values are means ± SEM of three separate experiments.
[b] SEM: Standard Error of the Mean.

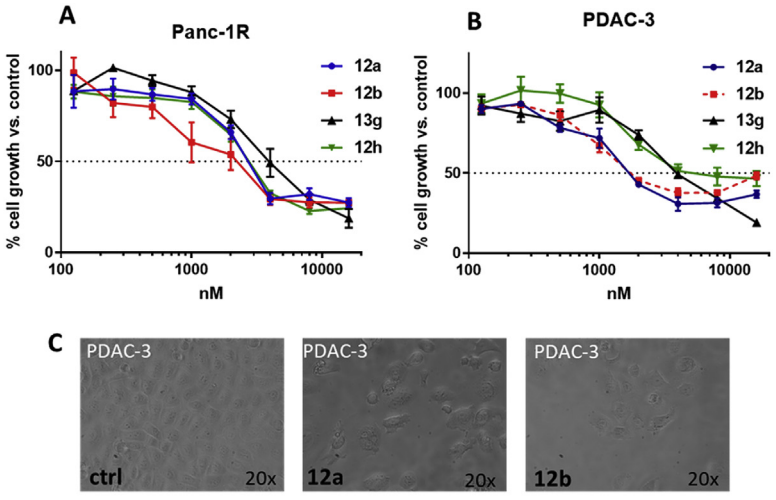

D

Cell line	12a	12b	12h	13g	Gemcitabine	5-fluorouracil
PDAC-3	1.7 ± 0.39	1.7 ± 0.27	5.1 ± 0.37	3.9 ± 0.18	0.03 ± 0.01	0.56 ± 0.32
Panc-1R	2.7 ± 0.25	2.2 ± 0.37	2.8 ± 0.3	3.9 ± 0.8	>10	4.5 ± 0.54

Fig. 4. Representative growth curves of Panc-1R (**A**) and PDAC-3 (**B**) cells treated with the compounds **12a,b,h** and **13g** (from 0.125 to 16 μM). *Points*, mean values obtained from three independent experiments; *bars*, SEM. (**C**) Representative pictures of PDAC-3 cells after 72 h from the treatment at concentration of IC_{50} value. *Left panel*: untreated cells; *central panel*: cells treated with compound **12a**; *right panel:* cells treated with compound **12b**. Original magnification 20X. (**D**) IC_{50} values of compounds **12a,b,h** and **13g** on gemcitabine-resistant and primary PDAC-3 cells ([a]The values are means of three separated experiments. [b]SEM: Standard Error Mean).

3.3. Reduction of cell migration

Next to the lack of clinically relevant improvement in effective treatments, the high metastatic potential of PDAC is one of the main causes for the poor outcome of this disease [36]. The ability of the compounds **12a** and **12b** to inhibit the migratory behaviour of PDAC cells was investigated by scratch wound-healing assays on SUIT-2, Capan-1, Panc-1, Panc-1R and PDAC-3 cell lines.

Briefly, 5 × 104 cells/well were seeded into 96-well flat-bottom plates in a volume of 100 μL and incubated for 24 h to create a monolayer. The scratches in the middle of the wells were created by scraping with a specific tool with needles. The cells were then treated with the compounds using 4x IC50 concentrations. These concentrations were chosen after preliminary experiments demonstrating that the exposure for 24 h did not result in pro-apoptotic or necrotic effects. The wound closure was monitored by phase-contrast microscopy and the pictures were captured immediately after scratch (T = 0), and at 4, 8, 20 and 24 h from the

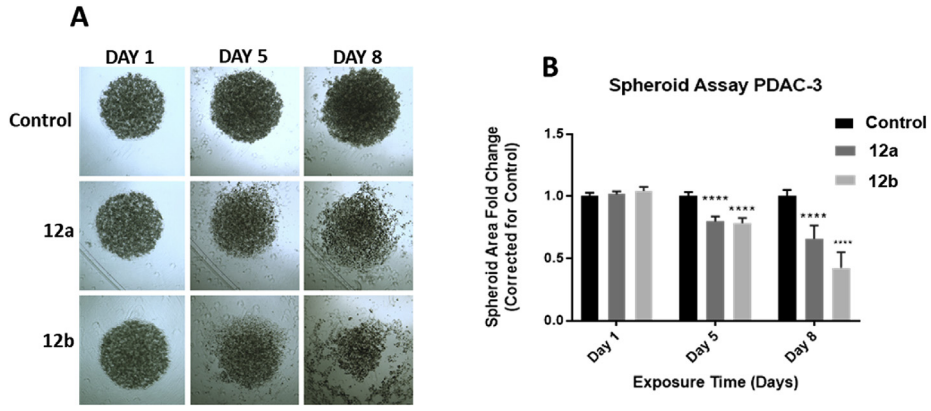

Fig. 5. Size reduction of PDAC-3 spheroids treated with compounds **12a** and **12 b** at 5-times the IC_{50} (i.e. 8.5 μM). (**A**) Representative pictures of PDAC-3 spheroids exposed to **12a** and **12b**, taken at day 1 of treatment, and after 5 and 8 days with an automated phase-contrast microscope. (**B**) Fold-change, corrected for control, of the spheroids size, at Day 1, Day 5 and Day 8. p-values were determined by Two-way ANOVA followed by Tukey's multiple comparisons test, **** = $p < 0.0001$. The values were obtained taking into account the mean values of the areas of at least ten different spheroids.

treatment. As shown in Fig. 6A–D, the compounds **12a** and **12b** induced a remarkable reduction of cell migration rate in Panc-1R and SUIT-2 cell lines. The scratch area (μm^2) was already wider in the treated cells compared to the untreated Panc-1R cells after 8 h of treatment. After 24 h from the beginning of the treatment we observed a reduction of the cell migration with a fold-change value of approximately 4 in both cell lines, SUIT-2 and Panc-1, treated with compounds **12a** and **12b** (Fig. 6A,B). Statistical analyses revealed that these differences were significant, compared to the respective controls (i.e., untreated cells) in both cell lines.

In particular, compared to untreated cells (set at 100%), the percentages of migration in cells treated with the compounds **12a** and **12b** were of 33.3% and 32%, respectively, in Panc-1R (Fig. 6C), and 34.9% and 41%, respectively, in SUIT-2 (Fig. 6D) after 24 h from the start of the treatment. The anti-migratory activity was also evident in Capan-1 and Panc-1 cells for which we observed similar statistically significant results, with migration rates between 50% and 60% (Fig. 7A–C and Fig. 7A–D). Finally, as shown in the Supplementary data Fig. 1A, we detected lower migration rates (64% and 71%, respectively) compared to the control (set at 100%) also in the primary PDAC-3 cells treated with the compounds **12a** and **12b**. Overall, these data highlighted the ability of our compounds to significantly reduce the rate of cell migration on all the PDAC preclinical models.

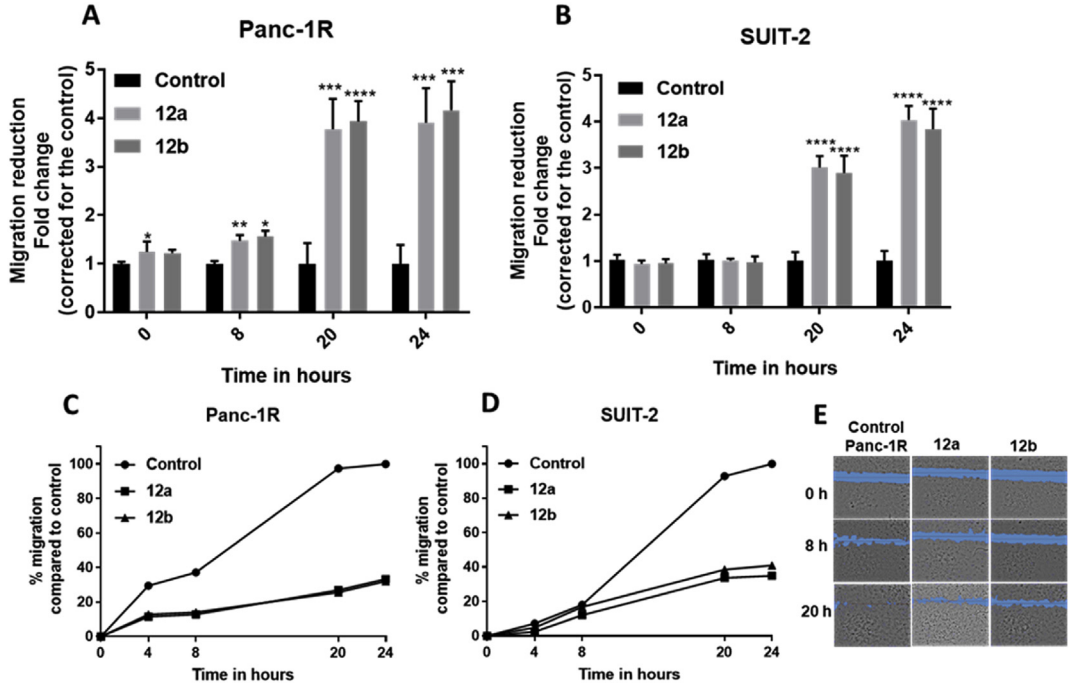

Fig. 6. Modulation of the migration rate in Panc-1R and SUIT-2 cells treated with the compounds **12a** and **12 b** at concentration of 4x IC50. (**A-B**) Fold-changes in Panc-1R (**A**) and SUIT-2 (**B**) cells were determined by taking into consideration at least four scratch areas. All the *P* values were calculated with Student's t-test. ****$p < 0.0001$, ***$p < 0.001$, **$p < 0.01$, *$p < 0.05$. (**C-D**) Percentages of migration monitored over time (0, 4, 8, 20 and 24 h) of Panc-1R (**C**) and SUIT-2 (**D**) cells treated with compound **12a** and **12 b** at concentration 4x IC50. *Points*, mean values obtained from the means of at least three different scratch areas. (**E**) Representative images of the wounds closure captured with the microscope at 0, 8 and 20 h on Panc-1R cells. Original magnification 5X.

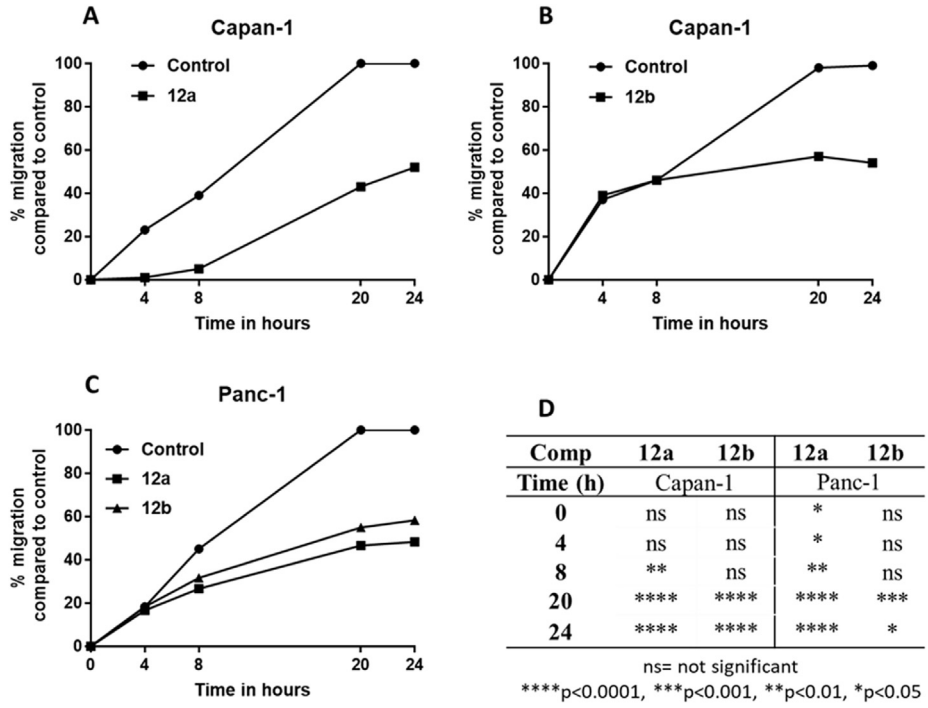

Fig. 7. (**A-D**) Percentage of migration monitored over time (0, 4, 8, 20 and 24 h) of Capan-1 (**A-B**) and Panc-1 (**C**) cells treated with the compounds **12a** and **12 b** at concentrations of 4x IC50. *Points*, mean values obtained from the means of at least three different scratch areas. (**D**) *(Table)* List of *P* values that were calculated with Student's t-test. ****$p < 0.0001$, ***$p < 0.001$, **$p < 0.01$, *$p < 0.05$, ns = not significant.

3.4. Modulation of epithelial mesenchymal transition events as assessed by qRT-PCR, western blot and gelatine zymography

It is well known that epithelial-to-mesenchymal transition (EMT) events are essential for embryonic development and other physiological events, such as the response to several injuries. During EMT, epithelial cells undergo changes in their phenotypic tracts through the loss of polarity, cell-cell adhesion and extracellular matrix, and they acquire mesenchymal features including motility and invasiveness [47]. Several transcription factors within the cellular microenvironment regulate the expression of epithelial and mesenchymal marker genes, among which the most important include the zinc finger transcription factors SNAIL1 and SNAIL2, potent epithelial repressors belonging to the SNAIL superfamily, E-cadherin (CDH1) and N-cadherin (CDH12), calcium-dependent cell adhesion molecules, vimentin (VIM), type III intermediate filament (IF) protein typically expressed in mesenchymal cells, and finally, the matrix metalloproteinases (MMPs), enzymes involved in the breakdown of extracellular matrix [48]. Remarkably, their dysregulation induces a transition from the physiological function to the pathological one, including mechanisms underlying the origin and progression of tumors and tissue fibrosis [49]. The loss of CDH1 expression is considered the hallmark of EMTs in cancer and recently, SNAIL1 and SNAIL2 have been identified as the major determinants for the repression of its transcription through the direct binding to the E-cadherin E-box promoter [50–52]. Simultaneously, the gain of mesenchymal markers, such as VIM, CDH12, MMPs and others occur [53]. In PDAC, these genes contribute to a crucial network of signalling pathways that contribute to the irreversible change of cell phenotype, both in metastasis and resistance to the chemotherapy [54]. Because of their outstanding effects against PDAC cell migration, we assessed the influence of the imidazothiadiazole derivatives **12a** and **12b** on these EMTs key regulator expression, in SUIT-2, Capan-1 and Panc-1 cells, using RT-qPCR, Western blot and gelatine zymography analyses. Capan-1 and SUIT-2 cells were selected for these experiments because preliminary analyses of the housekeeping protein GAPDH showed that using lysates of these cells the Western blot images were not "saturated" and were kept in the linear range (as revealed by exposing blots to increasing times and drawing a plot of intensity and time exposure). RT-qPCR reactions were performed in order to evaluate the modulation of the mRNA expression of SNAIL1, SNAIL2, CDH1, CDH12. Briefly, SUIT-2 and Capan-1 cells (2.5×10^5/well) were seeded into 6-well plates and incubated for 24 h to form a confluent monolayer. Then they were treated with the compounds **12a** and **12 b** at concentrations of 5x IC_{50}. After 24 h, the cells were harvested using TRIzol, and we extracted the total RNA, which was used to synthesize, by reverse transcription, the cDNA for the PCR reactions. The expression levels were normalized to those of the glyceraldehyde-3-phosphate dehydrogenase (GAPDH) housekeeping gene, whose expression was constant in all cells, as described previously [55]. As shown in Fig. 8A and B, the compounds **12a** and **12b** affected the genes leading EMTs. In both cell lines the mRNA levels of SNAIL1 and SNAIL2 were increased from 1.5 to approximately 1.9 fold compared to the GAPDH in the control cells, suggesting a low amount of protein expression and consequently, due to a negative feedback mechanism, CDH1 protein expression was upregulated, as reported in the Western blot analysis (Fig. 8C and D, Fig. 8G and Supplementary data Fig. 2). Instead, the protein expression of VIM and MMP2 were significantly reduced. Finally, CDH12 protein expression did not noticeably change compared to the control.

Furthermore, considering the pivotal role of MMPs in tumor invasion, through degradation of extracellular matrix components, we evaluated the effect of the compounds **12a** and **12b** on the proteolytic activity of MMP2 and MMP9 by using specific gelatine zymography assays. These assays showed a significant decrease of the activity of MMP2 and MMP9 isolated from SUIT-2 and Capan-

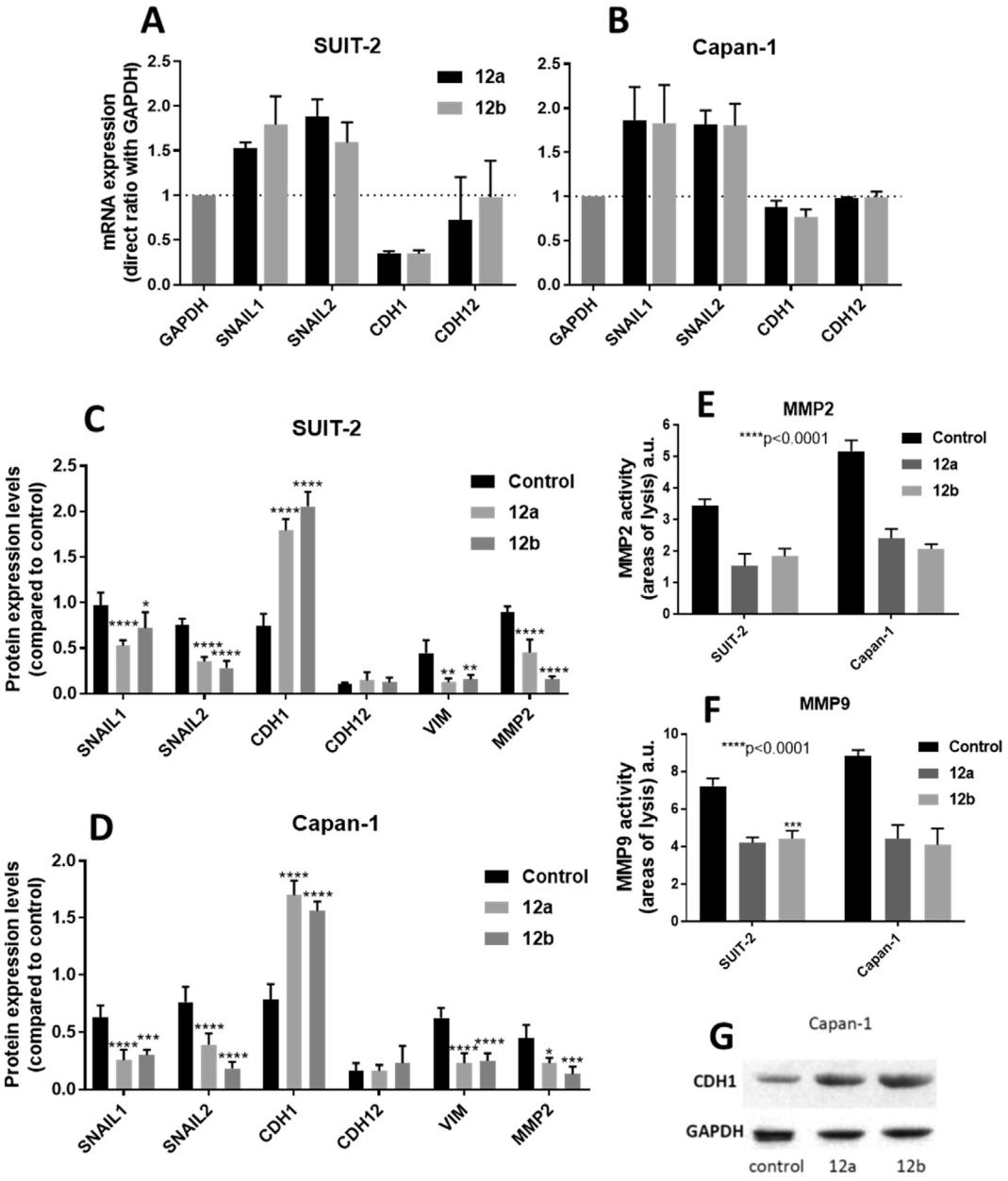

Fig. 8. SNAIL1, SNAIL2, CDH1 and CDH12 mRNA expressions in SUIT-2 (**A**) and Capan-1 (**B**) cells treated with the compounds **12a** and **12 b** at 5x IC_{50} for 24 h. The expression levels were determined by RT-qPCR and the results were obtained by the delta-delta Ct (cycle threshold) analysis. The experiments were conducted in duplicates and the values are shown as means ± SD. (**C-D**) SNAIL1, SNAIL2, CDH1, CDH12, VIM and MMP2 protein levels expression in SUIT-2 (**C**) and Capan-1 (**D**) cells treated with compounds **12a** and **12b**. The protein levels were determined after 24 h of treatment at concentration 5x IC_{50} value by densitometric analysis of the Western Blot performed using ImageJ. All the *P* values were determined by Tukey's multiple comparisons test. ****p < 0.0001, ***p < 0.001, **p < 0.01, *p < 0.05. (**E-F**) Gelatine zymography analysis of media from SUIT-2 and Capan-1 cells incubated with serum-free medium for 24 h. The enzymatic activity of MMP2 and MMP9 was determined by densitometric analysis. The cells were treated with the compounds **12a** and **12 b** at concentration 5x IC_{50} value for 24 h ****p < 0.0001, ***p < 0.001. (**G**) Representative image of CDH1 expression determined by Western blot analysis in Capan-1 cells treated with the compounds **12a** and **12 b** at 5x IC_{50} concentrations after 24 h.

1 cells exposed to the compounds. In particular, the activities of the MMP2 and MMP9 enzymes were decreased by about 50% after 24 h of treatment compared to the control (Fig. 8E and F). However, as shown in the Supplementary data Fig. 3, the areas of lysis created by the proteolytic activities of both enzymes isolated from Panc-1 cells treated with compounds **12a** and **12b** were not significantly wider compared to the control.

3.5. Profiling of inhibition of kinase activity

To investigate the potential mechanism of action of our compounds, we performed a high-throughput analysis with the Pamgene tyrosine kinase peptide substrate array (PamChip). The PamChip consists of 4 identical arrays, each of which contains 144 peptide sequences immobilized on a porous ceramic membrane (Fig. 9A). Each of these sequences harbours one or more phosphorylation sites, derived from literature or computational predictions. Finally, specific fluorescently labelled anti-phospho antibodies are used to detect the amount of phosphorylated protein by tyrosine kinases from our samples.

The compound **12b** significantly inhibited the phosphorylation of 45 peptide substrates in SUIT-2 cells, and we visualized on

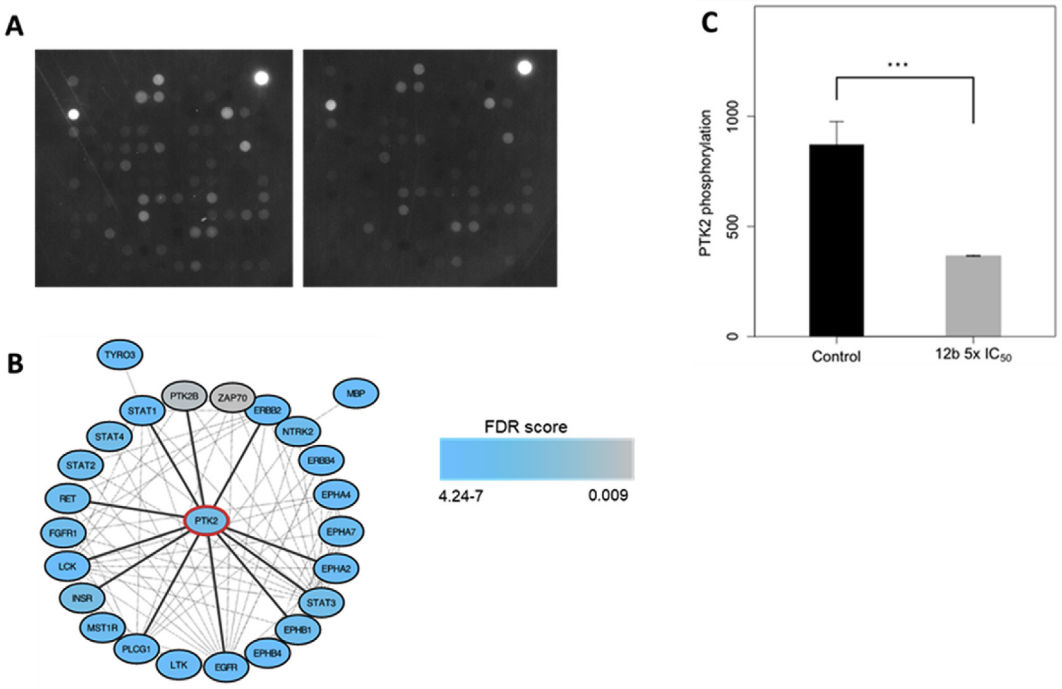

Fig. 9. (**A**) Representative images of pictures taken at the end point of the control array (left) and the treated array (right). (**B**) Network visualization obtained with Cytoscape of the significant proteins containing differentially phosphorylated peptides, color legend indicates the significance level of each protein. (**C**) Barplot of PTK2 phosphorylation in the control vs treated with 5x IC_{50} of **12b**. (For interpretation of the references to color in this figure legend, the reader is referred to the Web version of this article.)

Cytoscape a network highlighting the interactions between proteins containing the phosphorylated peptides. Notably, PTK2/FAK emerged as an important hub between those proteins (Fig. 9B). In particular, the phosphorylation of PTK2/FAK showed a more than 2-fold inhibition after treatment with compound **12b**, with FDR <0.01 (Fig. 9C). This result prompted us to validate the inhibition of phosphorylation of PTK2/FAK as one of the possible mechanisms of action of our compound, using a specific ELISA assay, as detailed in the following paragraphs.

3.6. Inhibition of PTK2/FAK as assessed by ELISA

The focal adhesion kinase (FAK), also known as protein tyrosine kinase 2 (PTK2), is a downstream non-receptor tyrosine kinase able to mediate information from extracellular matrix into the cytoplasmatic compartment, through a linker with intracellular tails of integrins [56]. FAK controls several cellular processes, including survival, proliferation and motility. However, its overexpression is correlated with many aspects of the tumorigenesis. For instance, FAK regulates the development of metastasis, driving adhesion, invasion and migration events. Furthermore, the translocation of FAK in the nucleus induces the arrest of p53 activity and its downstream gene transcription [57]. In PDAC, FAK coordinates several signalling pathways involved in growth and metastasis processes [58]. Notably, a recent study reported the ability of the indole-3-carbinol to affect EMTs genes and reduce FAK mRNA expression in MCF-7 cells [59]. Thereby, we conducted a quantitative analysis by the Enzyme-Linked Immunosorbent Assay (ELISA) to investigate whether our imidazothiadiazole compounds could reduce FAK phosphorylation at tyrosine residue 397 (FAK [pY397]), which is essential for the kinase activity of this protein. This assay was carried out on lysates of SUIT-2, Capan-1 and Panc-1 cells treated with compounds **12a** and **12 b** at concentrations of 5x IC_{50s} for 24 h. As shown in Fig. 10, these ELISA experiments showed a reduction of p-FAK in all the PDAC cell lines, with fold-change values ranging from 0.4 to 0.5. Similar results were observed in the Western blot analyses of the same compounds (Supplementary Fig. 4). These results suggest that FAK is a target of our compounds and might explain how they can then suppress FAK-driven migration, and growth in PDAC cells.

4. Conclusions

A new series of hybrid molecules, **12a,b,d,e,f,h, 13c,g,i,j** and **14k-r** compounds bearing in the same structure the imidazo [2,1-*b*] [1,3,4]thiadiazole and indole scaffolds were efficiently synthesized and evaluated for their antiproliferative activity and mechanism of action on a panel of PDAC cells, namely SUIT-2, Capan-1 and Panc-1.

Among the synthesized imidazothiadiazoles, compounds **12a,b,d,e,f,h, 13c,g,i,j** and **14k,l,n,o,p** were screened by the NCI on the full panel of sixty human cancer cells at concentration of 10 μM. Notably, compounds **12a** and **12h** displayed relevant antiproliferative activity eliciting GI_{50} values in the range from micro-to sub-micromolar levels. In addition, compounds **12b** and **13g** considerably reduced PDAC cell proliferation in SUIT-2, Capan-1, Panc-1, Panc-1R (gemcitabine-resistant) and in the primary cells PDAC-3, growing as monolayers or as spheroids. Noteworthy, compounds **12a,b,h** and **13g** are characterized by a thiophene ring at position 6 of the imidazothiadiazole scaffold, suggesting the importance of this ring for the pharmacological activity. However, in order to confirm the role of aldehyde for the antiproliferative activity future studies in **14a-j** compounds are warranted.

Through wound-healing assays we found remarkably reduction of cell migration in all the PDAC preclinical models when treated with the most promising compounds **12a** and **12b**. These effects might be explained by modulation of key regulators of EMT, including E-cadherin and vimentin, as well as by the inhibition of MMP-2/-9 activities. Finally, high-throughput analysis with kinase arrays revealed a significant inhibition of the phosphorylation of 45 tyrosine kinases substrates, whose visualization on Cytoscape

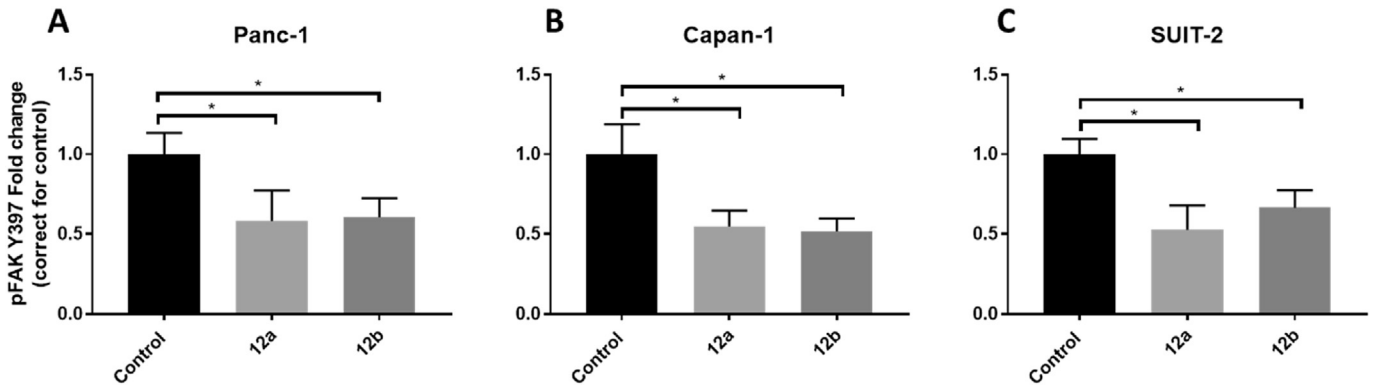

Fig. 10. Inhibition of FAK/PTK2 phosphorylation by compounds **12a** and **12b.** Modulation of phosphorylated-FAK (pFAK) at tyrosine residue 397 by compounds **12a** and **12b** on Panc-1 (**A**), Capan-1 (**B**) and SUIT-2 (**C**) cells. The amount of pFAK was measured in cell lysates after 24 h from the treatment with compounds **12a** and **12 b** at 5x IC_{50s}. All the *P* values were calculated with Student's t-test, $^{*}p < 0.05$.

highlighted PTK2/FAK as an important hub between those proteins. These results were validated using a specific ELISA assay, which demonstrated the inhibition of phosphorylation of PTK2/FAK. Altogether these results support the high potential of this type of compounds against EMT and PTK2/FAK, which play a key role in the aggressiveness of pancreatic cancer [55]. In order to support our experimental findings we also investigated the molecular structure of FAK. Unfortunately complete crystal structures of the molecule are not available; e.g. the Tyr397 part is lacking in the published structures, which may be due to the high flexibility of this region of the molecule. This means that proper molecular docking is not yet feasible.

5. Experimental section

5.1. Chemistry

All melting points were taken on a Büchi-Tottoly capillary apparatus and are uncorrected. IR spectra were determined in bromoform with a Shimadzu FT/IR 8400S spectrophotometer. ^{1}H and ^{13}C NMR spectra were measured at 200 and 50.0 MHz, respectively, in DMSO-d_6 solution, using a Bruker Avance II series 200 MHz spectrometer. Column chromatography was performed with Merck silica gel 230–400 mesh ASTM or with Büchi Sepacor chromatography module (prepacked cartridge system). Elemental analyses (C, H, N) were within ±0.4% of theoretical values and were performed with a VARIO EL III elemental analyzer. The LC/HRMS have been obtained on a Thermo Q-Exactive system equipped with a Dionex 3000 chromatographic system.

5.1.1. Synthesis of 1H-indole-3-carbonitriles (**9b-e**)

A solution of the suitable indole **8** (5.10 mmol) in anhydrous acetonitrile (4.5 mL) was treated dropwise with chlorosulfonyl isocyanate (CSI) (0.44 mL, 5.10 mmol). The reaction mixture was maintained at 0 °C under stirring for 2 h, then, anhydrous dimethylformamide (DMF) (2.8 mL, 36.39 mmol) was slowly added and the mixture was stirred at 0 °C for 1.5 h. The resulting solution was poured into crushed ice. The solid obtained was filtered and dried (yields 98–100%). Analytical and spectroscopic data for compounds **9b-e** are in agreement with those previously reported [60].

5.1.2. Synthesis of 1-methylindole-3-carbonitriles (**10a-e**)

To a solution of the suitable 3-cyanoindole **9** (7.03 mmol) in anhydrous DMF (10 mL) 3.61 mmol of K_2CO_3 and dimethyl carbonate (1.8 mL, 21.4 mmol) were added and the mixture was heated at 130 °C for 3.5 h. After cooling (0–5 °C), water and ice (25 mL) was slowly added under stirring. The oily suspension obtained was extracted with diethyl ether (3 × 10 mL), the organic phase was washed with water and brine, dried over Na_2SO_4 and the solvent evaporated at reduced pressure to obtain the 3-cyano-1-methylindoles **10** in excellent yields. Analytical and spectroscopic data are in accordance to those reported in literature [16].

5.1.3. Synthesis of 5-(1H-indol-3-yl)-1,3,4-thiadiazol-2-amines (**11a-j**)

A mixture of the suitable indole-3-carbonitrile **9a-e** or **10a-e** (5 mmol), thiosemicarbazide (5 mmol) and trifluoroacetic acid (5 mL) was heated under stirring at 60 °C for 3.5 h. The reaction mixture was then poured into ice and neutralized with $NaHCO_3$ saturated solution. The solid obtained was filtered off, washed with water, cyclohexane and diethyl ether to give 5-(1*H*-indol-3-yl)-1,3,4-thiadiazol-2-amines **11a-j** in excellent yields. Analytical and spectroscopic data for the derivatives **11a-f** are in accordance to those reported in literature [16].

*5.1.3.1. 5-(5-Methoxy-1H-indol-3-yl)-1,3,4-thiadiazol-2-amine (**11g**).* Light yellow solid. Yield: 98%, m.p. 216–217 °C IR: 3604 (NH), 3558 (NH_2) cm^{-1}; ^{1}HNMR (200 MHz, DMSO-d_6) δ: 3.79 (3H, s, CH_3), 6.88 (1H, dd, $J = 2.4$, 8.8 Hz, Ar–H), 7.39 (1H, d, $J = 8.8$ Hz, Ar–H), 7.53 (1H, d, $J = 2.3$ Hz, Ar–H), 8.02 (1H, s, Ar–H), 8.58 (2H, bs, NH_2), 12.07 (1H, bs, NH). ^{13}C NMR (50 MHz, DMSO-d_6) δ: 55.2 (q), 101.9 (d), 105.7 (s), 112.9 (d), 113.0 (d), 124.4 (s), 128.7 (d), 131.5 (s), 152.2 (s), 154.7 (s), 166.5 (s). Anal. Calcd for $C_{11}H_{10}N_4OS$ (MW: 246.29): C, 53.64; H, 4.09; N, 22.75. Found: C, 53.72; H, 4.16; N, 22.98.

*5.1.3.2. 5-(5-Methoxy-1-methyl-1H-indol-3-yl)-1,3,4-thiadiazol-2-amine (**11h**).* Light yellow solid. Yield: 99%, m.p. 205–206 °C IR: 3381 (NH_2) cm^{-1}; ^{1}HNMR (200 MHz, DMSO-d_6) δ: 3.80 (6H, s, CH_3, OCH_3), 6.90 (1H, dd, $J = 2.5$, 8.8 Hz, Ar–H), 7.13 (2H, s, NH_2), 7.41 (1H, d, $J = 8.9$ Hz, Ar–H), 7.61 (1H, d, $J = 2.4$ Hz, Ar–H), 7.81 (1H, s, Ar–H). ^{13}C NMR (50 MHz, DMSO-d_6) δ: 32.8 (q), 55.3 (q), 102.3 (d), 106.0 (s), 111.2 (d), 112.5 (d), 124.9 (s), 130.7 (d), 132.0 (s), 152.2 (s), 154.6 (s), 165.4 (s). Anal. Calcd for $C_{12}H_{12}N_4OS$ (MW: 260.31): C, 55.37; H, 4.65; N, 21.52. Found: C, 55.42; H, 4.80; N, 21.78.

*5.1.3.3. 5-(5-Fluoro-1H-indol-3-yl)-1,3,4-thiadiazol-2-amine (**11i**).* Light yellow solid. Yield: 98%, m.p. 257 °C IR: 3609 (NH), 3461 (NH_2) cm^{-1}; ^{1}HNMR (200 MHz, DMSO-d_6) δ: 7.03–7.12 (1H, m, Ar–H), 7.33–750 (3H, m, Ar–H, NH_2), 7.80 (1H, dd, $J = 2.5$, 10.0 Hz, Ar–H), 7.95 (1H, s, Ar–H), 11.79 (1H, s, NH). ^{13}C NMR (50 MHz, DMSO-d_6) δ: 105.4 (d, $J = 24$ Hz), 107.4 (s, $J = 4.5$ Hz), 110.7 (d, $J = 25.5$ Hz), 113.1 (d, $J = 10$ Hz), 124.4 (s, $J = 11$ Hz), 128.6 (d), 130.1 (s), 152.0 (s), 159.9

(s), 165.9 (s). Anal. Calcd for $C_{10}H_7FN_4S$ (MW: 234.25): C, 51.27; H, 3.01; N, 23.92. Found: C, 51.38; H, 3.25; N, 24.12.

*5.1.3.4. 5-(5-Fluoro-1-methyl-1H-indol-3-yl)-1,3,4-thiadiazol-2-amine (**11j**).* Light orange solid. Yield: 98%, m.p. 183 °C. IR: 3471 (NH_2) cm $^{-1}$; ^{1}HNMR (200 MHz, DMSO-d_6) δ: 3.85 (3H, s, CH_3), 7.12–7.21 (1H, m, Ar–H), 7.59 (1H, dd, J = 4.4, 9.9 Hz, Ar–H), 7.76 (2H, dd, J = 2.5, 9.8 Hz, Ar–H), 8.10 (2H, s, NH_2). ^{13}C NMR (50 MHz, DMSO-d_6) δ: 33.14 (q), 105.4 (s), 105.5 (d, J = 24 Hz), 110.9 (d, J = 26 Hz), 112.0 (d, J = 9.5 Hz), 124.3 (s), 124.5 (s), 133.1 (d), 151.4 (s), 155.7 (s). Anal. Calcd for $C_{11}H_9FN_4S$ (MW: 248.28): C, 53.21; H, 3.65; N, 22.57. Found: C, 53.38; H, 3.88; N, 22.72.

*5.1.4. General procedure for the synthesis of 3-(6-phenylimidazo [2,1-b] [1,3,4]thiadiazol-2-yl)-1H-indole derivatives (**12** and **13**)*

A mixture of 5-(1*H*-indol-3-yl)-1,3,4-thiadiazol-2-amine **11a-j** (0.92 mmol) and the suitable α-bromoacetyl derivative (0.92 mmol) in 40 mL of anhydrous ethanol was stirred at reflux for 24 h. After cooling at room temperature the desired product **12** was filtered off and washed with cold ethanol.

Derivatives **12a**,**b**,**d**-**f**,**h** were isolated as pure compounds and were characterized without further purifications. Whereas, compounds **12c**,**g**,**i**,**j** were treated with saturated aqueous $NaHCO_3$ solution to give the corresponding free bases **13** which were purified by silica gel column chromatography eluting by petroleum ether:-ethyl acetate, 1:1. Analytical and spectroscopic data for the derivatives **12k-r** are in accordance to those reported in literature [16].

*5.1.4.1. 3-[6-(Thiophen-3-yl)imidazo[2,1-b] [1,3,4]thiadiazol-2-yl]-1H-indole hydrobromide (**12a**).* White solid, yield: 57%, m.p. 288–289 °C, IR cm^{-1}: 3630 (NH), 3458 (NH). ^{1}HNMR (200 MHz, DMSO-d_6) δ: 7.27–7.34 (2H, m, 2xAr-H), 7.54–7.59 (2H, m, 2xAr-H), 7.68 (1H, dd, J = 2.9, 5.0 Hz, Ar–H), 7.89 (1H, dd, J = 1.1, 2.8 Hz, Ar–H), 8.16 (1H, dd, J = 2.8, 6.2 Hz, Ar–H), 8.42 (1H, d, J = 3.0 Hz, Ar–H), 8.71 (1H, s, Ar–H), 10.63 (1H, bs, NH), 12.24 (1H, s, NH). ^{13}C NMR (50 MHz, DMSO-d_6) δ: 106.06 (s), 110.68 (d), 112.62 (d), 120.30 (d), 120.52 (d), 121.65 (d), 123.31 (d), 123.71 (s), 125.47 (d), 127.24 (d), 130.00 (d), 133.78 (s), 136.70 (s), 139.17 (s), 142.45 (s), 158.13 (s). Anal. Calcd for $C_{16}H_{11}BrN_4S_2$ (MW: 403.32): C, 47.65; H, 2.75; N, 13.89. Found: C, 47.74; H, 2.83; N, 13.95. LC-HRMS: 323.04979 m/z.

*5.1.4.2. 1-Methyl-3-[6-(thiophen-3-yl)imidazo[2,1-b] [1,3,4]thiadiazol-2-yl]-1H-indole hydrobromide (**12b**).* Greenish yellow solid, yield: 55%, m.p. 317–318 °C, IR cm^{-1}: 2650 (NH). ^{1}HNMR (200 MHz, DMSO-d_6) δ: 3.91 (3H, s, CH_3), 6.50 (1H, bs, NH), 7.32–7.41 (2H, m, 2xAr-H), 7.55 (1H, d, J = 4.9 Hz, Ar–H),7.61–7.66 (2H, m, 3xAr-H), 7.81 (1H, d, J = 2.4 Hz, Ar–H), 8.16 (1H, dd, J = 2.4, 6.2 Hz, Ar–H), 8.38 (1H, s, Ar–H), 8.60 (1H, s, Ar–H). ^{13}C NMR (50 MHz, DMSO-d_6) δ: 33.14 (q), 99.50 (s), 105.39 (s), 110.30 (d), 111.01 (d), 119.59 (d), 120.44 (s), 121.77 (d), 123.23 (d), 124.06 (s), 125.53 (d), 126.74 (d), 132.95 (s), 133.28 (d), 135.53 (s), 137.25 (s), 141.09 (d). Anal. Calcd for $C_{17}H_{13}BrN_4S_2$ (MW: 417.35): C, 48.92; H, 3.14; N, 13.42. Found: C, 48.85; H, 3.22; N, 13.51. LC-HRMS: 337.05688 m/z.

*5.1.4.3. 5-Bromo-1-methyl-3-[6-(thiophen-3-yl)imidazo[2,1-b] [1,3,4]thiadiazol-2-yl]-1H-indole hydrobromide (**12d**).* Whitish solid, yield: 68%, m.p. 318–319 °C, IR cm^{-1}: 2697–2500 (NH). ^{1}HNMR (200 MHz, DMSO-d_6) δ: 3.87 (3H, s, CH_3), 7.43–7.68 (4H, m, Ar–H), 7.81–7.83 (1H, m, Ar–H), 8.24 (1H, d, J = 1.76 Hz, Ar–H), 8.38 (1H, bs, NH), 8.43 (1H, s, Ar–H), 8.69 (1H, s, Ar–H). ^{13}C NMR (50 MHz, DMSO-d_6) δ: 33.39 (q), 104.55 (s), 110.72 (d), 113.26 (d), 114.60 (s), 120.41 (d), 122.63 (d), 125.38 (d), 125.49 (s), 125.80 (d), 127.21 (d), 133.90 (s), 134.58 (d), 136.01 (s), 139.42 (s), 142.21 (s), 157.02 (s). Anal. Calcd for $C_{17}H_{12}Br_2N_4S_2$ (MW: 496.24): C, 41.15H, 2.44; N, 11.29. Found: C, 41.22; H, 2.52; N, 11.41. LC-HRMS: 416.96634 m/z.

*5.1.4.4. 5-Chloro-3-[6-(thiophen-3-yl)imidazo[2,1-b] [1,3,4]thiadiazol-2-yl]-1H-indole hydrobromide (**12e**).* Whitish solid, yield: 63%, m.p. 276–277 °C, IR cm^{-1}: 3285 (NH), 3168 (NH). ^{1}HNMR (200 MHz, DMSO-d_6) δ: 7.32 (1H, d, J = 2.1 Hz, Ar–H), 7.52–7.68 (3H, m, Ar–H), 7.83 (1H, m, Ar–H), 8.15 (1H, d, J = 1.9 Hz, Ar–H), 8.46 (1H, d, J = 2.9 Hz, Ar–H), 8.71 (1H, s, Ar–H), 9.19 (1H, bs, NH), 12.37 (1H, s, NH). ^{13}C NMR (50 MHz, DMSO-d_6) δ: 92.15 (s), 99.49 (s), 106.10 (s), 110.43 (d), 114.24 (d), 119.58 (d), 120.27 (d), 121.37 (s), 123.35 (d), 124.74 (s), 125.80 (d), 126.17 (s), 126.67 (d), 131.35 (d), 134.16 (s), 135.22 (s). Anal. Calcd for $C_{16}H_{10}BrClN_4S_2$ (MW: 437.76): C, 43.90; H, 2.30; N, 12.80. Found: C, 43.99; H, 2.41; N, 12.91. LC-HRMS: 357.00452 m/z.

*5.1.4.5. 5-Chloro-1-methyl-3-[6-(thiophen-3-yl)imidazo[2,1-b] [1,3,4]thiadiazol-2-yl]-1H-indole hydrobromide (**12f**).* Whitish solid, yield: 68%, m.p. 324–325 °C, IR cm^{-1}: 2625–2496 (NH). ^{1}HNMR (200 MHz, DMSO-d_6) δ: 3.87(3H, s, CH_3), 7.36 (1H, d, J = 2.0 Hz Ar–H), 7.51 (1H, m, J = 4.5 Hz Ar–H), 7.60–7.68 (2H, m, Ar–H), 7.82 (1H, d, J = 1.8 Hz, Ar–H), 8.07 (1H, d, J = 1.9 Hz, Ar–H), 8.45 (1H, s, Ar–H), 8.64 (1H, bs, NH), 8.68 (1H, s, Ar–H). ^{13}C NMR (50 MHz, DMSO-d_6) δ: 33.41 (q), 104.61 (s), 110.72 (d), 112.84 (d), 119.60 (d), 120.50 (d), 123.24 (d), 124.87 (s), 125.38 (d), 126.61 (s), 127.23 (d), 133.73 (s), 134.73 (d), 135.75 (s), 139.26 (s), 142.19 (s), 157.10 (s). Anal. Calcd for $C_{17}H_{12}BrClN_4S_2$ (MW: 451.79): C, 45.19; H, 2.68; N, 12.40. Found: C, 45.25; H, 2.74; N, 12.45. LC-HRMS: 371.02017 m/z.

*5.1.4.6. 5-Fluoro-1-methyl-3-[6-(thiophen-3-yl)imidazo[2,1-b] [1,3,4]thiadiazol-2-yl]-1H-indole hydro-bromide (**12h**).* White solid, yield: 58%, m.p. 286–287 °C, IR cm^{-1}: 2713–2485 (NH). ^{1}HNMR (200 MHz, DMSO-d_6) δ: 3.88 (3H, s, CH_3), 7.20 (1H, td, J = 2.4, 9.2 Hz, Ar–H), 7.54 (1H, d, J = 5.0 Hz, Ar–H), 7.59–7.69 (2H, m, Ar–H), 7.78 (1H, dd, J = 2.3, 9.6 Hz, Ar–H), 7.86 (1H, d, J = 2.3 Hz, Ar–H), 8.47 (1H, s, Ar–H), 8.67 (1H, s, Ar–H), 10.04 (H, bs, NH). ^{13}C NMR (50 MHz, DMSO-d_6) δ: 33.50 (q), 104.74 (d), 104.83 (s), 105.35 (d, J = 6.2 Hz), 110.73 (d), 111.45 (d, J = 26.1 Hz), 112.65 (d, J = 26.1 Hz), 120.84 (d), 124.15 (s), 124.37 (s), 125.39 (d), 127.36 (s), 133.08 (s), 133.93 (s), 135.03 (d), 140.25 (s, J = 180.3 Hz), 157.62 (s). Anal. Calcd for $C_{17}H_{12}BrFN_4S_2$ (MW: 435.33): C, 46.90; H, 2.78; N, 12.87. Found: C, 47.01; H, 2.87; N, 12.95. LC-HRMS: 355.04926 m/z.

*5.1.4.7. 5-Bromo-3-[6-(thiophen-3-yl)imidazo[2,1-b] [1,3,4]thiadiazol-2-yl]-1H-indole (**13c**).* Whitish solid, yield: 58%, m.p. 299–300 °C, IR cm^{-1}: 3535–3633 (NH). ^{1}HNMR (200 MHz, DMSO-d_6) δ: 7.39–7.44 (1H, m, Ar–H), 7.50–7.54 (2H, m, Ar–H), 7.59–7.63 (1H, m, Ar–H), 7.75 (1H, dd, J = 1.1, 1.1 Hz, Ar–H), 8.32 (2H, d, J = 1.7 Hz, Ar–H), 8.60 (1H, s, Ar–H), 12.29 (1H, s, NH). ^{13}C NMR (50 MHz, DMSO-d_6) δ: 99.49 (s), 106.21 (s), 110.38 (d), 114.03 (s), 114.59 (d), 119.34 (d), 122.61 (d), 125.46 (d), 125.77 (d), 126.72 (d), 130.65 (d), 135.45 (s), 135.98 (s), 141.65 (s), 142.62 (s), 156.42 (s). Anal. Calcd for $C_{16}H_9BrN_4S_2$ (MW: 401.30): C, 47.89; H, 2.26; N, 13.96. Found: C, 47.95; H, 2.31; N, 14.04. LC-HRMS: 402.95081 m/z.

*5.1.4.8. 5-Fluoro-3-[6-(thiophen-3-yl)imidazo[2,1-b] [1,3,4]thiadiazol-2-yl]-1H-indole (**13g**).* Yellow solid, yield: 80%, m.p. 260–261 °C, IR cm^{-1}: 3630 (NH). ^{1}HNMR (200 MHz, DMSO-d_6) δ: 7.16 (1H, td, J = 2.5, 9.2 Hz, Ar–H), 7.52–7.63 (3H, m, 3xAr-H), 7.75–7.77 (1H, m, Ar–H), 7.84 (1H, dd, J = 2.4, 9.8 Hz, Ar–H), 8.38 (1H, d, J = 2.9 Hz, Ar–H), 8.55 (1H, s, Ar–H), 12.24 (1H, s, NH). ^{13}C NMR (50 MHz, DMSO-d_6) δ: 99.40 (s), 104.61 (s), 105.78 (s), 111.36 (d), 113.77 (s), 120.20 (d), 123.70 (s), 123.96 (s), 126.46 (d), 128.11 (d), 131.63 (s), 133.24 (s), 135.45 (d), 138.25 (d), 140.74 (d), 145.68 (d). Anal. Calcd for $C_{16}H_9FN_4S_2$ (MW: 340.4): C, 56.45; H, 2.66; N, 16.46. Found: C, 56.51; H, 2.71; N, 16.56. LC-HRMS: 341.03256 m/z.

*5.1.4.9. 5-Methoxy-3-[6-(thiophen-3-yl)imidazo[2,1-b] [1,3,4]thiadiazol-2-yl]-1H-indole (**13i**).* Yellow solid, yield: 58%, m.p. 255–256 °C, IR cm^{-1}: 3628 (NH). ^{1}HNMR (200 MHz, DMSO-d_6) δ: 3.85 (3H, s, CH_3), 6.95 (1H, dd, J = 2.4, 8.8 Hz, Ar–H), 7.44 (1H, d, J = 8.8 Hz, Ar–H), 7.52–7.65 (3H, m, Ar–H), 7.75 (1H, dd, J = 1.0, 2.8 Hz Ar–H), 8.24 (1H, d, J = 3.0 Hz, Ar–H), 8.55 (1H, s, Ar–H), 12.00 (1H, s, NH). ^{13}C NMR (50 MHz, DMSO-d_6) δ: 55.32 (q), 102.18 (d), 106.35 (s), 110.30 (d), 113.09 (d), 113.30 (d), 119.24 (d), 124.34 (s), 125.52 (d), 126.66 (d), 129.59 (d), 131.61 (s), 136.07 (s), 141.49 (s), 142.55 (s), 155.09 (s), 157.08 (s). Anal. Calcd for $C_{17}H_{12}N_4OS_2$ (MW: 352.43): C, 57.93; H, 3.43; N, 15.90. Found: C, 57.88; H, 3.52; N, 15.99. LC-HRMS: 353.05377 m/z.

*5.1.4.10. 5-Methoxy-1-methyl-3-[6-(thiophen-3-yl)imidazo[2,1-b] [1,3,4]thiadiazol-2-yl]-1H-indole (**13j**).* Yellow solid, yield: 60%, m.p. 213–214 °C, ^{1}HNMR (200 MHz, DMSO-d_6) δ: 3.86 (6H, s, OCH_3, CH_3), 6.99 (1H, dd, J = 2.5, 7.7 Hz, Ar–H), 7.50–7.64 (4H, m, Ar–H), 7.75 (1H, d, J = 3.2 Hz, Ar–H), 8.26 (1H, s, Ar–H), 8.55 (1H, s, Ar–H). ^{13}C NMR (50 MHz, DMSO-d_6) δ: 33.24 (q, CH_3), 55.38 (q, CH_3), 99.49 (s), 102.32 (d), 105.06 (s), 110.35 (d), 111.90 (d), 112.96 (d), 119.24 (d), 124.61 (s), 125.52 (d), 126.67 (d), 132.30 (s), 133.03 (d), 136.00 (s), 141.46 (s), 142.43 (s), 155.37 (s), 156.63 (s). Anal. Calcd for $C_{18}H_{14}N_4OS_2$ (MW: 366.46): C, 58.99; H, 3.85; N, 15.29. Found: C, 59.07; H, 3.91; N, 15.37. LC-HRMS: 367.06955 m/z.

*5.1.5. General procedure for the synthesis 2-(1H-indol-3-yl)-6-phenylimidazo[2,1-b] [1,3,4]thiadiazole-5-carbaldehydes **14k-r***

Vilsmeier reagent was prepared at 0 °C by adding dropwise $POCl_3$ (0.11 mL) into a stirred DMF anhydrous (0.08 mL). The appropriate derivative **13** (0.5 mmol) in 2 mL of DMF anhydrous was added and the solution was heated at 70 °C under stirring for 5h. The reaction mixture was poured onto ice and the corresponding aldehyde **14** was filtered off and purified by silica gel column chromatography eluting by petroleum ether:ethyl acetate, 3:7.

Derivatives **14l, 14q** were characterized only by ^{1}HNMR spectra due to their poor solubility.

*5.1.5.1. 2-(1H-indol-3-yl)-6-phenylimidazo[2,1-b] [1,3,4]thiadiazole-5-carbaldehyde (**14k**).* White solid, yield: 70%, m.p. 285–286 °C, IR cm^{-1}: 2918 (NH), 1683 (CO). ^{1}HNMR (200 MHz, DMSO-d_6) δ: 7.30 (1H, m, Ar–H), 7.52 (2H, d, J = 6.8 Hz, Ar–H), 8.01 (2H, d, J = 5.8 Hz, Ar–H), 8.27–8.30 (3H, m, Ar–H), 8.41 (2H, d, J = 3.0 Hz, Ar–H), 10.08 (1H, s, CHO), 12.20 (1H, s, NH). ^{13}C NMR (50 MHz, DMSO-d_6) δ: 106.20 (s), 112.64 (d), 120.65 (d), 121.70 (d), 123.36 (d), 123.47 (s), 123.80 (s), 128.67 (4xd), 129.41 (d), 130.10 (d), 132.38 (s), 136.68 (s), 148.53 (s), 153.45 (s), 159.38 (s), 177.31 (d). Anal. Calcd for $C_{19}H_{12}N_4OS$ (MW: 344.39): C, 66.26; H, 3.51; N, 16.27. Found: C, 66.35; H, 3.59; N, 16.41. LC-HRMS: 345.08148 m/z.

*5.1.5.2. 2-(1-Methyl-1H-indol-3-yl)-6-phenylimidazo[2,1-b] [1,3,4]thiadiazole-5-carbaldehyde (**14l**).* White solid, yield: 91%, m.p. 233–234 °C, IR cm^{-1}: 1560 (CO). ^{1}HNMR (200 MHz, DMSO-d_6) δ: 3.90 (3H, s, CH_3), 7.31–7.59 (6H, m, Ar–H), 7.87–8.41(4H, m, Ar–H), 10.07 (1H, s, CHO). Anal. Calcd for $C_{20}H_{14}N_4OS$ (MW: 358.4): Composition: C, 67.02; H, 3.94; N, 15.63. Found: C, 67.28; H, 4.11; N, 15.75. LC-HRMS: 214.09023 m/z.

*5.1.5.3. 6-(4-Fluorophenyl)-2-(1H-indol-3-yl)imidazo[2,1-b] [1,3,4]thiadiazole-5-carbaldehyde (**14m**).* White solid, yield: 81%, m.p. 255–256 °C, IR cm^{-1}:3158 (NH), 1560 (CO). ^{1}HNMR (200 MHz, DMSO-d_6) δ: 7.28–7.38 (4H, m, Ar–H), 7.52–7.55 (1H, m, Ar–H), 8.08–8.11 (2H, m, Ar–H), 8.26–8.29 (1H, m, Ar–H), 8.40 (1H, s, Ar–H), 10.09 (1H, s, CHO), 12.19 (1H, s, NH). ^{13}C NMR (50 MHz, DMSO-d_6) δ: 99.5 (s), 106.1 (s), 112.5 (d), 115.3 (d), 115.8 (d), 120.6 (d), 121.7 (d), 123.3 (d), 123.8 (2xs), 128.9 (s), 130.2 (d), 130.7 (d), 130.9 (d), 136.7 (s), 148.2 (s), 151.8 (s), 159.4 (s), 177.3 (d). Anal. Calcd for $C_{19}H_{11}FN_4OS$ (MW: 362.38): C, 62.97; H, 3.06; N, 15.46. Found: C, 63.05; H, 3.11; N, 15.53. LC-HRMS: 363.07043 m/z.

*5.1.5.4. 2-(1H-indol-3-yl)-6-(3-methoxyphenyl)imidazo[2,1-b] [1,3,4] thiadiazole-5-carbaldehyde (**14n**).* White solid, yield: 60%, m.p. 278–279 °C, IR cm^{-1}: 3308 (NH), 1560 (CO). ^{1}HNMR (200 MHz, DMSO-d_6) δ: 3.84 (3H, s, CH_3), 7.06 (1H, d, J = 6.7 Hz, Ar–H), 7.29–7.32 (2H, m, Ar–H), 7.41–7.46 (1H, m, Ar–H), 7.55 (1H, dd, J = 3.1, 5.8 Hz, Ar–H), 7.61 (2H, m, Ar–H), 8.30 (1H, m, Ar–H), 8.42 (1H, d, Ar–H), 10.10 (1H, s, CHO), 12.20 (1H, s, NH). ^{13}C NMR (50 MHz, DMSO-d_6) δ: 55.2 (q), 99.49 (s), 106.2 (s), 113.5 (2xd), 120.7 (d), 121.0 (d), 121.7 (d), 123.3 (d), 123.6 (s), 123.8 (s), 129.7 (2xd), 130.1 (d), 133.7 (s), 136.7 (s), 153.0 (s), 159.3 (s), 159.4 (s), 177.3 (d). Anal. Calcd for $C_{20}H_{14}N_4O_2S$ (MW: 374.42): C, 64.16; H, 3.77; N, 14.96. Found: C, 64.25; H, 3.51; N, 15.13. LC-HRMS: 375.09232 m/z.

*5.1.5.5. 6-(2,5-Dimethoxyphenyl)-2-(1H-indol-3-yl)imidazo[2,1-b] [1,3,4]thiadiazole-5-carbaldehyde (**14o**).* Yellow solid, yield: 82%, m.p. 268–269 °C, IR cm^{-1}: 1561 (CO). ^{1}HNMR (200 MHz, DMSO-d_6) δ: 3.75 (3H, s, CH_3), 3.77 (3H, s, CH_3), 7.02–7.18 (3H, m, Ar–H), 7.32 (2H, dd, J = 2.9, 5.8 Hz, Ar–H), 7.55–7.58 (1H, m, Ar–H), 8.28 (2H, d, J = 5.5 Hz, Ar–H), 8.42 (1H, s, Ar–H), 9.76 (1H, s, CHO), 12.21 (1H, s, NH). ^{13}C NMR (50 MHz, DMSO-d_6) δ: 55.5 (q), 55.9 (q), 99.5 (s), 106.2 (s), 112.5 (d), 113.1 (d), 116.1 (d), 116.3 (2xd), 120.62 (s), 121.7 (d), 122.1 (s), 123.3 (d), 123.8 (s), 130.0 (d), 136.7 (s), 148.7 (s), 150.4 (s), 153.1 (s), 159.2 (s), 177.6 (d). Anal. Calcd for $C_{21}H_{16}N_4O_3S$ (MW: 404.44): C, 62.36; H, 3.99; N, 13.85. Found: C, 62.49; H, 4.05; N, 13.63. LC-HRMS: 405.10297 m/z.

*5.1.5.6. 6-(2,5-Dimethoxyphenyl)-2-(1-methyl-1H-indol-3-yl)imidazo[2,1-b] [1,3,4]thiadiazole-5-carbaldehyde (**14p**).* White solid, yield: 70%, m.p. 216–217 °C, IR cm^{-1}: 1667 (CO). ^{1}HNMR (200 MHz, DMSO-d_6) δ: 3.75 (3H, s, CH_3), 3.77 (3H, s, CH_3), 3.92 (3H, s, CH_3), 7.06 (1H, dd, J = 2.9, 5.8 Hz, Ar–H), 7.17 (2H, m, Ar–H), 7.36–7.39 (2H, t, J = 4.0 Hz, Ar–H), 7.64 (1H, d, J = 8.8 Hz, Ar–H), 8.27 (1H, d, J = 10.4 Hz, Ar–H), 8.43 (1H, s, Ar–H), 9.76 (1H, s, CHO). ^{13}C NMR (50 MHz, DMSO-d_6) δ: 33.2 (q), 55.5 (q), 55.97 (q), 99.5 (s), 105.1 (s), 108.5 (d), 111.1 (d), 113.1 (d), 116.1 (s), 116.3 (d), 118.73 (d), 120.68 (d), 122.0 (d), 123.4 (d), 123.9 (s), 124.1 (s),136.2 (s),137.3 (s), 148.6 (s), 150.4 (s), 153.0 (s), 158.8 (s), 177.6 (d). Anal. Calcd for $C_{22}H_{18}N_4O_3S$ (MW: 418.47): C, 63.14; H, 4.34; N, 13.39. Found: C, 63.21; H, 4.43; N, 13.48. LC-HRMS: 419.11682 m/z.

*5.1.5.7. 2-(1H-indol-3-yl)-6-(4-nitrophenyl)imidazo[2,1-b] [1,3,4] thiadiazole-5-carbaldehyde (**14q**).* Yellow solid, yield: 75%, m.p. 314–315 °C, IR cm^{-1}: 3311 (NH), 1561 (CO). ^{1}HNMR (200 MHz, DMSO-d_6) δ: 7.31 (2H, d, J = 2.9 Hz, Ar–H), 7.52 (1H, s, Ar–H), 8.34–8.43 (5H, m, Ar–H), 10.21 (1H, s, CHO), 12.23 (1H, s, NH). Anal. Calcd for $C_{19}H_{11}N_5O_3S$ (MW: 389.39): C, 58.61; H, 2.85; N, 17.99. Found: C, 58.82; H, 2.73; N, 18.09. LC-HRMS: 390.06683 m/z.

*5.1.5.8. 2-(5-Bromo-1H-indol-3-yl)-6-(2,5-dimethoxyphenyl)imidazo[2,1-b] [1,3,4]thiadiazole-5-carbaldehyde (**14r**).* White solid, yield: 90%, m.p. 250–251 °C, IR cm^{-1}: 3268 (NH), 1654 (CO). ^{1}HNMR (200 MHz, DMSO-d_6) δ: 3.76 (6H, d, J = 3.9 Hz, 2xCH_3), 7.08–7.18 (3H, m, Ar–H), 7.42–7.56 (2H, m, Ar–H), 8.45 (2H, d, J = 10.3 Hz, Ar–H), 9.76 (1H, s, CHO), 12.38 (1H, bs, NH). ^{13}C NMR (50 MHz, DMSO-d_6) δ: 55.3 (q), 55.9 (q), 99.5 (s), 105.9 (s), 108.2 (s), 114.3 (s), 116.1 (d), 116.3 (d), 122.0 (s), 122.9 (d), 123.9 (s), 125.5 (s), 126.0 (d), 131.2 (d), 135.5 (s), 141.6 (d), 150.3 (s), 150.7 (d), 153.3 (s), 158.7 (s), 178.6 (d). Anal. Calcd for $C_{21}H_{15}BrN_4O_3S$ (MW: 483.33): C, 52.18; H, 3.13; N, 11.59. Found: C, 52.39; H, 3.21; N, 11.70. LC-HRMS: 485.01031 m/z.

5.2. Biology

5.2.1. Drugs and chemicals

The synthesized imidazothiadiazole compounds **12**–**14** were dissolved in DMSO. The medium, foetal bovine serum (FBS), penicillin (50 IU mL^{-1}) and streptomycin (50 μg mL^{-1}) were from Gibco (Gaithersburg, MD, USA). All other chemicals were from Sigma (Zwijndrecht, the Netherlands).

5.2.2. Cell culture

Capan-1 and Panc-1 cell lines, were purchased at the ATCC (Manassas, VA, USA), while SUIT-2 cells were a generous gift from Dr. Adam Frampton (Imperial College, London, UK). Panc-1R cells, a gemcitabine-resistant sub-clone obtained by continuous incubation of Panc-1 with 1 μM of this drug, were achieved as described previously [41]. The primary PDAC-3 culture was isolated from a patient at Pisa Hospital as described previously [61]. The cell lines were tested for their authentication by STR–PCR, performed by BaseClear (Leiden, the Netherlands). The cells were cultured in RPMI-1640 (Roswell Park Memorial Institute 1640) supplemented with 10% heat-inactivated FBS, 1% penicillin/streptomycin, or in DMEM (Dulbecco's Modified Eagle's Medium), supplemented with 10% heat-inactivated FBS, 1% HEPES. The cells were kept in a humidified atmosphere of 5% CO_2 and 95% air at 37 °C and harvested with trypsin-EDTA. Not all these preclinical models allowed to perform the different experiments to check antitumor properties of new compounds. In particular, PDAC-3 cells were selected to form spheroids which are more representative of the aggregation of tumor cells in vivo, as also reported in our previous studies. All the PDAC cells, i.e., Panc-1R, SUIT-2 and PDAC-3, but also Panc-1 and Capan-1 cells were selected for the wound-healing assay because in all these cells the exposure for 24 h with our compounds did not result in pro-apoptotic or necrotic effects, allowing a reliable analysis of the results. Capan-1 and SUIT-2 cells were selected for Western blot, zymography and PCR assays because preliminary analyses of the housekeeping protein GAPDH at the Western blot showed that using lysates of these cells the Western blot images were not "saturated" and were kept in the linear range (as revealed by exposing blots to increasing times and drawing a plot of intensity and time exposure). SUIT-2 cells were selected for the PamChip array because of the lowest background noise observed in preliminary experiments.

5.2.3. Cell growth inhibition

The *in vitro* antiproliferative activity of the new imidazothiadiazole compounds **12a,b,d,e,f,h**, **13c,g,i,j** and **14k-r** was evaluated on a panel of pancreatic cancer cells by Sulforhodamine-B (SRB) assay, both for primary cell cultures (PDAC-3) and for the immortalized cell lines (SUIT-2, Capan-1, Panc-1 and Panc-1R), following a previously described protocol [42]. The cytotoxicity of the new compounds **12a** and **12b** was also evaluated in the normal fibroblast cells Hs27. The results of these experiments allowed us to calculate the selectivity index (SI, IC_{50} non-tumor cell line/IC_{50} tumor cell line).

Cells were seeded into a 96-well flat-bottom plates in triplicate in a volume of 100 μL (3×10^3 cells/well for SUIT-2, Panc-1, Panc-1R and PDAC-3 cell lines, 5×10^3 cells/well for Capan-1 cells, and 8×10^3 cells/well for Hs27 cells) and incubated for 24 h at 37 °C to create a confluent monolayer. Then, the cells were treated with 100 μL of the compounds dissolved in DMSO at different concentration (125–16000 nM) for 72 h at 37 °C, 5% CO_2 and 100% humidity. At the end of incubation period, the cells were fixed with 25 μL of 50% cold trichloroacetic acid (TCA) and kept for at least 60 min at 4 °C. Then, the plates were emptied and washed gently with deionized water, dried at room temperature (RT) overnight and stained with 50 μL of 0.4% SRB solution in 1% acetic acid for 15 min at RT. The excess of SRB stain was removed and the plates were washed with a 1% acetic acid solution and let dry at RT overnight. The SRB staining was dissolved in 150 μL of tris(hydroxymethyl)aminomethane solution pH = 8.8 (TRIS base), and the absorbance was measured at wavelengths of 490 nm and 540 nm. Cell growth inhibition was calculated as the percentage of drug treated cells versus vehicle-treated cells ("untreated cells or control") OD (corrected for OD before drug addiction, "day-0"). The 50% inhibitory concentration of cell growth (IC_{50}) was calculated by non-linear least squares curve fitting (GraphPad PRISM, Intuitive Software for Science, San Diego, CA). In the NCI protocol IC_{50} is named GI_{50} (50% growth inhibitory concentration).

5.2.4. Wound-healing assay

The *in vitro* scratch wound-healing assay was performed as previously described [62]. SUIT-2, Capan-1, Panc-1 and Panc-1R cells were seeded in 96-well flat-bottom plates at the density of 5×104 cells/well in 100 μL. After 24 h of pre-incubation at 37 °C, 5% CO_2 and 100% humidity, the cell monolayers were scratched using a specific tool with multiple needles to create scratches of constant width. After removal of the detached cells by washing with phosphate buffered saline (PBS) solution, in the control wells the medium was replaced with only medium while the medium added with the compounds of interest in the experimental wells. The wound confluence was monitored by phase-contrast microscopy (Universal Grab 6.3 software, Digital Cell Imaging Labs, Keerbergen, Belgium) integrated to the Leica DMI300B (Leica Microsystems, Eindhoven, Netherlands) migration station and the pictures were captured immediately after scratch (T = 0), and 4, 8, 20 and 24 h from the treatment. The results were analyzed with the Scratch Assay 6.2 software (Digital Cell Imaging Labs).

5.2.5. Spheroid assay

PDAC-3 spheroids were grown in CELLSTAR®96-well cell repellent U-bottom plates (Greiner Bio-One, Cat No. 650970, Kremsmünster, Austria). Cells were seeded at the density of 2×10^4 cells per well, and incubated at 37 °C, 5% CO_2 for 72 h in order to let the spheroids form.

Before the treatment a picture of the plate was taken with an automated phase-contrast microscope DMI300B (Leica Microsystems, Eindhoven, Netherlands), and the subsequent pictures were taken every two days. After 72 h of incubation the culture medium was replaced with medium added with compounds of interest, which were diluted to the final concentration of 8.5 μM (5x the IC_{50}, obtained with previous growth-inhibition assay). Despite the careful pipetting, tilting the plate and placing the pipette tip on the side of the well, the structure of the spheroid was disturbed so we decided to centrifuge the plate at 200xRCF, for 3 min at RT (Rotixa 500RS, Hettich Zentrifugen Technology, Tuttlingen, Germany). The treatment was repeated after four days, to ensure the availability of nutrients, and so was the centrifuge.

Pictures were analyzed with ImageJ Software (U.S. National Institute of Health, Bethesda, Maryland, USA) to determine the area of the spheroids treated and compare it to the area of the untreated spheroids, as described previously [63].

5.2.6. RNA isolation

RNA was extracted from SUIT-2, Capan-1 and Panc-1 cells according to TRIzol-chloroform protocol as described previously [64]. Cells were seeded in a 6-well plate in a density of 2.5×10^5 cells/well and kept at 37 °C, with a constant level of CO_2 (5%) and 100% humidity for 24 h. Subsequently, the cells were treated for 24 h with the compounds of interest at concentration 5x IC_{50} and stored for an additional 24 h in the incubator. The cells were then

harvested by 250 μL of TRIzol reagent. After precipitation with isopropanol and washing with 70% ethanol, the total RNA appeared as a white gel-like pellet at the bottom of the tube. RNA yields and integrity were determined by measuring optical density at 260 nm with a Thermo Scientific NanoDrop 1000™ Spectrophotometer, controlled by ND1000 software. Instead, the test for detection of contaminations by protein or by organic compounds, thiocyanates and phenolate ions was performed by measuring absorbance at 280 and 230 nm, respectively.

5.2.7. Reverse transcription (RT) and quantitative real-time PCR (qRT-PCR)

For qRT-PCR, complementary DNA (cDNA) synthesis was performed according to manufacturer's protocol Thermo Scientific™ First Strand cDNA Synthesis Kit. For the reverse transcriptase reactions, 1.5 μg of mRNA was added to a 1 μL of random hexamer primer and, finally, water nuclease free up to a final volume of 11 μL. Therefore, 5X Reaction Buffer (4 μL), RiboLock RNase Inhibitor (20 U/μL) (1 μL), 10 nM dNTP Mix (2 μL) and M-MuLV Reverse Transcriptase (20 U/μL) (2 μL) components were added (all provided by Kit). The mixture was incubated for 5 min at 25 °C followed by 60 min at 37 °C. Subsequently, the reaction was terminated by heating at 70 °C for 5 min. The DNA samples obtained (20 μL) were diluted 1:10 and used immediately for the RT-PCR assay. RT-PCR reactions were performed using the commercial TaqMan® Universal PCR Master Mix kit. For the RT-PCR, 25 μL of total mix per well is needed. Therefore, 12.5 μL of Universal Master Mix 2X (AmpliTaq Gold DNA Polymerase, dNTPs with dUTP, passive reference, and optimized buffer components), 1 μL of Primers and TaqMan® probe, 6.5 μL of H_2O and 5 μL of cDNA sample were loaded in duplicate on a 96-well PCR plate and the amplification was carried out in a GeneAmp 5700 Sequence Detection System. Samples were amplified by following the thermal cycle conditions for 40 cycles: an initial incubation at 50°C for 2 min to prevent the reamplification of carry-over PCR products by AmpErase uracil-N-glycosylase, followed by incubation at 95°C for 10 min to suppress AmpErase UNG activity and denature the DNA, followed by annealing and extension at 60 °C for 1 min. Primers and probes were obtained from Applied Biosystems Assay-on Demand Gene expression products to amplify the following genes: *SNAIL1* (Hs00195591_m1), *SNAIL2* (Hs00950344_m1), *CDH1* (Hs010 23894_m1), *CDH12* (Hs00362037_m1). GAPDH (Hs02758991_g1) has been used as housekeeping gene to normalize the amplifications. All reactions were performed in duplicate using the ABI PRISM7500 sequence detection system instrument (AppliedBiosystems). The cycle threshold (Ct) was determined and gene expression levels relative to that of GAPDH were calculated by the $2^{-\Delta\Delta CT}$ method, as described previously.

5.2.8. Western blot and gelatine zymography

The protein expression of SNAIL1, SNAIL2, CDH1, CDH12, and VIM in SUIT-2, PANC-1 and Capan-1 cells treated with compounds 12a and 12b was evaluated by Western Blot analysis as described previously [65]. All the primary antibodies were from Cell Signalling Technology (Beverly, MA). Additional Western blot analyses were performed in order to evaluate the phosphorylation of FAK, using the Phospho-FAK (Tyr397) Antibody #3283 (Cell Signalling Technology).

The activity of MMP2 and MMP9 was evaluated by gelatine zymography, as described previously [65]. PDAC cells (10^6) were seeded in Petri dishes and incubated with serum-free medium for 24 h, with or without the selected compounds at 5x IC_{50}. Medium was harvested and centrifuged (1500 rpm for 5 min) in order to remove cellular debris. The collected media were then mixed with SDS-PAGE buffer 4X without reducing agent and underwent electrophoresis in 10% polyacrylamide gel containing 1 mg/mL gelatine. After 1 h, the gel was exposed to renaturating buffer (50 mM Tris-HCl pH 7, 6.5 mM $CaCl_2$, 1 μM $ZnCl_2$, 2.5% Triton X-100) for 15 min, washed with washing buffer (50 mM Tris-HCl pH 7, 6.5 mM $CaCl_2$, 1 μM $ZnCl_2$) and finally incubated with developing buffer (50 mM Tris-HCl pH 7, 6.5 mM $CaCl_2$, 1 μM $ZnCl_2$, 1% Triton X-100, 0.02% NaN_3) for 16 h at 37 °C. The staining was then performed using 0.25% Coomassie Brilliant Blue R-250 solution containing 45% methanol and 10% glacial acetic acid for 4 h, washed with a solution of 10% glacial acetic acid and 45% methanol for 2 h. The areas of protease activity were detected as clear bands and the activity of MMPs was assessed by densitometric scanning and quantitative analysis using ImageJ software (National Institutes of Health, Bethesda, MD, US).

5.2.9. PamChip® kinase activity profiling

A PamChip array with 144 kinase peptides substrates (#86312 PamGene International B.V., 's-Hertogenbosch, The Netherlands) was used to test the change in tyrosine kinase activity when using the **12b** compound. This experiment was performed with SUIT-2 cells in biological duplicates (two untreated samples and two treated samples with **12b** compound), as described previously [66,67].

5.2.10. Preparation of cell lysates

Cells were grown in 25 cm^2 flasks until they reached 80% of confluence, at 37 °C and 5% of CO_2, then SUIT-2 cells were treated with 5 μM of **12b** (5x IC_{50}), and the medium of control cells was replaced with fresh medium. Treatment lasted 24 h, and then cells were lysed with 100 μL x 10^6 cells of M-PER lysis buffer containing: M-PER Mammalian Extraction Buffer (Thermo Scientific, Rockford, IL, USA), Halt protease Inhibitor cocktail, EDTA free (Complete Mini EDTA-free Protease Inhibitor Cocktail, Roche #11836170001), Halt Phosphatase Inhibitor Cocktail (Thermo Fisher #78420) both diluted 1:100, for at least 15 min at 4 °C. The lysates were collected in 1.5 mL tubes, which were centrifuged (at 4 °C, 16000g) for 15 min, and the supernatants were collected and stored at −80 °C until use. Protein concentration of the samples was determined using Bio-Rad protein Assay, based on the method of Bradford (Bio-Rad, Hercules, CA).

5.2.11. Tyrosine kinase activity profiling

Lysates for the PamChips were prepared in order to reach a concentration of 10 μg protein/array, and they were added to the MasterMix (PamGene reagent kit 32116) containing: PK buffer 10x, BSA solution 100x, PTK additive 10x, 1 M DTT solution, Complete Mini EDTA-free Protease Inhibitor Cocktail, Halt Phosphatase Inhibitor Cocktail 400x (Thermo Fisher), PY-20-FITC (fluorescent labelled antibody), 4 mM ATP solution. Samples were added to the MasterMix immediately prior to loading on the chip. Before loading the samples, the PamStation®12 instrument performed a blocking step with 25 μL of 2% BSA on each array followed by three wash steps with PK buffer, then 40 μL of each sample mix was loaded in duplicate onto the arrays. During incubation at 30 °C, the sample mix was pumped up and down through the array once per minute for 60 cycles. Repeated fluorescent imaging of each array was performed with a 12-bit CCD camera, monitoring fluorescence intensities in real time.

5.2.12. PamGene data analysis

The intensity of each spot at the end point was evaluated through an open source software (ScanAnalyze) and subsequently corrected for local background noise. Since the negative control was a negative value, all the intensities were subjected to a minimal shift to have the negative control equal to zero.

One duplicate of the treated samples was excluded from the analysis due to bad quality data ending with two controls and one treated samples. To maintain a balance and statistical power for the differential analysis, one extra sample for the control group was generated using the median of the two samples and adding a constant *k* while 2 extra samples for the treated group were generated adding a different constant *k* to the treated sample.

The differential analysis was performed by a Student *t*-test in R (version 3.6.1) and the p.value was corrected by FDR. The significant peptides were selected applying a cutoff on FDR <0.01. Visualization of differentially phosphorylated protein was performed in Cytoscape (version 3.5.0) and the barplot for PTK2 phosphorylation was generated in R (version 3.6.1).

5.2.13. Enzyme-Linked Immunosorbent Assay (ELISA) for phosphorylated FAK (pFAK) kinase

The pFAK level at tyrosine residue 397 was detected and quantified using Enzyme-Linked Immunosorbent Assay (ELISA). The assay was conducted using Invitrogen™ FAK [pY397] ELISA Kit (Cat. # KHO0441) according to the manufacturer's protocol. Supernatants from Panc-1, Capan-1 and SUIT-2 cells were collected after 24 h from the treatment with imidazothiadiazole compounds **12a** and **12 b** at concentration 5x IC_{50} value. The absorbance was read at 450 nm. We performed a parallel ELISA test using the well-known FAK inhibitor defactinib (5 μM). This drug reduced the FAK/PTK2 phosphorylation of 65%, supporting the use of this method in order to check the inhibition of pFAK.

5.2.14. Statistics

All SRB, PCR, Western blot, and zymography assays were carried out in triplicate and repeated at least three times, whereas the percentages of cell migration were calculated taking into account at least six scratch areas. The data was evaluated using the GraphPad Prism version 7 software (GraphPad Software, San Diego, CA, USA). Data is expressed as mean values ± SEM and analyzed by the Student *t*-test.

Declaration of competing interest

The authors declare that they have no known competing financial interests or personal relationships that could have appeared to influence the work reported in this paper.

Acknowledgments

This work was partially supported in the collections and analysis of data by the following grants: CCA Foundation 2015 and 2018 grants, KWF Dutch Cancer Society grants (KWF project#10401 and #11957) and AIRC/Start-Up grant (to E.G.). The Authors would like to thank Btissame El Hassouni, MSc (VUmc, Amsterdam, The Netherlands) for the support with the work on the cell culture experiments.

We thank the members of the Drug Discovery Commitee of the EORTC-PAMM group for the useful discussion and support.

Appendix A. Supplementary data

Supplementary data to this article can be found online at https://doi.org/10.1016/j.ejmech.2020.112088.

List of abbreviations

CDH1	E-cadherin
CDH12	N-cadherin
CSI	chlorosulfonyl isocyanate
DMF	Dimethylformamide
DMPM	diffuse malignant peritoneal mesothelioma
DMSO	Dimethyl sulfoxide
ELISA	enzyme-linked immunosorbent assay
EMT	epithelial mesenchymal transition
FAK	focal adhesion kinase
FBS	foetal bovine serum
FDR	false discovery rate
GI_{50}	growth inhibition of 50% of cells
IC_{50}	inhibitory concentration 50%
MMP-2/9	matrix metalloproteinases-2/9
NCI	National Cancer Institute
PDAC	pancreatic ductal adenocarcinoma
PTK2	protein tyrosine kinase 2
RT	room temperature
SD	standard deviation
SEM	standard error media
SI	selectivity index
SNAIL-1/2	zinc finger protein-1/2
TGI	total growth inhibition
VIM	vimentin

References

[1] K. Nepali, S. Sharma, M. Sharma, P.M.S. Bedi, K.L. Dhar, Rational approaches, design strategies, structure activity relationship and mechanistic insights for anticancer hybrids, Eur. J. Med. Chem. 77 (2014) 422–487, https://doi.org/10.1016/j.ejmech.2014.03.018.

[2] C. Viegas-Junior, A. Danuello, V. da Silva Bolzani, E.J. Barreiro, C.A.M. Fraga, Molecular hybridization: a useful tool in the design of new drug prototypes, Curr. Med. Chem. 14 (2007) 1829–1852.

[3] S. Nekkanti, R. Tokala, N. Shankaraiah, Targeting DNA minor groove by hybrid molecules as anticancer agents, Curr. Med. Chem. 24 (2017) 2887–2907, https://doi.org/10.2174/0929867324666170523102730.

[4] N. Kerru, P. Singh, N. Koorbanally, R. Raj, V. Kumar, Recent advances (2015-2016) in anticancer hybrids, Eur. J. Med. Chem. 142 (2017) 179–212, https://doi.org/10.1016/j.ejmech.2017.07.033.

[5] K. Yang, L. Fu, Mechanisms of resistance to BCR-ABL TKIs and the therapeutic strategies: a review, Crit. Rev. Oncol. Hematol. 93 (2015) 277–292, https://doi.org/10.1016/j.critrevonc.2014.11.001.

[6] P. Singla, V. Luxami, K. Paul, Synthesis and in vitro evaluation of novel triazine analogues as anticancer agents and their interaction studies with bovine serum albumin, Eur. J. Med. Chem. 117 (2016) 59–69, https://doi.org/10.1016/j.ejmech.2016.03.088.

[7] L.-Y. Ma, B. Wang, L.-P. Pang, M. Zhang, S.-Q. Wang, Y.-C. Zheng, K.-P. Shao, D.-Q. Xue, H.-M. Liu, Design and synthesis of novel 1,2,3-triazole-pyrimidine-urea hybrids as potential anticancer agents, Bioorg. Med. Chem. Lett 25 (2015) 1124–1128, https://doi.org/10.1016/j.bmcl.2014.12.087.

[8] H.-L. Qin, Z.-P. Shang, I. Jantan, O.U. Tan, M.A. Hussain, M. Sher, S.N.A. Bukhari, Molecular docking studies and biological evaluation of chalcone based pyrazolines as tyrosinase inhibitors and potential anticancer agents, RSC Adv. 5 (2015) 46330–46338, https://doi.org/10.1039/C5RA02995C.

[9] R. Romagnoli, P.G. Baraldi, F. Prencipe, J. Balzarini, S. Liekens, F. Estévez, Design, synthesis and antiproliferative activity of novel heterobivalent hybrids based on imidazo[2,1-b][1,3,4]thiadiazole and imidazo[2,1-b][1,3]thiazole scaffolds, Eur. J. Med. Chem. 101 (2015) 205–217, https://doi.org/10.1016/j.ejmech.2015.06.042.

[10] V.B. Jadhav, M.V. Kulkarni, V.P. Rasal, S.S. Biradar, M.D. Vinay, Synthesis and anti-inflammatory evaluation of methylene bridged benzofuranyl imidazo [2,1-b][1,3,4]thiadiazoles, Eur. J. Med. Chem. 43 (2008) 1721–1729, https://doi.org/10.1016/j.ejmech.2007.06.023.

[11] A. Tahghighi, S. Razmi, M. Mahdavi, P. Foroumadi, S.K. Ardestani, S. Emami, F. Kobarfard, S. Dastmalchi, A. Shafiee, A. Foroumadi, Synthesis and anti-leishmanial activity of 5-(5-nitrofuran-2-yl)-1,3,4-thiadiazol-2-amines containing N-[(1-benzyl-1H-1,2,3-triazol-4-yl)methyl] moieties, Eur. J. Med. Chem. 50 (2012) 124–128, https://doi.org/10.1016/j.ejmech.2012.01.046.

[12] K. Jakovljević, I.Z. Matić, T. Stanojković, A. Krivokuća, V. Marković, M.D. Joksović, N. Mihailović, M. Nićiforović, L. Joksović, Synthesis, antioxidant and antiproliferative activities of 1,3,4-thiadiazoles derived from phenolic acids, Bioorg. Med. Chem. Lett 27 (2017) 3709–3715, https://doi.org/10.1016/j.bmcl.2017.07.003.

[13] S.G. Alegaon, K.R. Alagawadi, P.V. Sonkusare, S.M. Chaudhary, D.H. Dadwe, A.S. Shah, Novel imidazo[2,1-b][1,3,4]thiadiazole carrying rhodanine-3-acetic acid as potential antitubercular agents, Bioorg. Med. Chem. Lett 22 (2012) 1917–1921, https://doi.org/10.1016/j.bmcl.2012.01.052.

[14] B.A. Bhongade, S. Talath, R.A. Gadad, A.K. Gadad, Biological activities of imidazo[2,1-b][1,3,4]thiadiazole derivatives: a review, J. Saudi Chem. Soc. 20

(2016) S463–S475, https://doi.org/10.1016/j.jscs.2013.01.010.
[15] D. Schillaci, V. Spanò, B. Parrino, A. Carbone, A. Montalbano, P. Barraja, P. Diana, G. Cirrincione, S. Cascioferro, Pharmaceutical approaches to target antibiotic resistance mechanisms, J. Med. Chem. 60 (2017) 8268–8297, https://doi.org/10.1021/acs.jmedchem.7b00215.
[16] S. Cascioferro, B. Parrino, G.L. Petri, M.G. Cusimano, D. Schillaci, V. Di Sarno, S. Musella, E. Giovannetti, G. Cirrincione, P. Diana, 2,6-Disubstituted imidazo [2,1-b][1,3,4]thiadiazole derivatives as potent staphylococcal biofilm inhibitors, Eur. J. Med. Chem. 167 (2019) 200–210, https://doi.org/10.1016/j.ejmech.2019.02.007.
[17] H.M. Patel, B. Sing, V. Bhardwaj, M. Palkar, M.S. Shaikh, R. Rane, W.S. Alwan, A.K. Gadad, M.N. Noolvi, R. Karpoormath, Design, synthesis and evaluation of small molecule imidazo[2,1-b][1,3,4]thiadiazoles as inhibitors of transforming growth factor-β type-I receptor kinase (ALK5), Eur. J. Med. Chem. 93 (2015) 599–613, https://doi.org/10.1016/j.ejmech.2014.09.002.
[18] S. Kumar, M. Hegde, V. Gopalakrishnan, V.K. Renuka, S.A. Ramareddy, E. De Clercq, D. Schols, A.K. Gudibabande Narasimhamurthy, S.C. Raghavan, S.S. Karki, 2-(4-Chlorobenzyl)-6-arylimidazo[2,1-b][1,3,4]thiadiazoles: synthesis, cytotoxic activity and mechanism of action, Eur. J. Med. Chem. 84 (2014) 687–697, https://doi.org/10.1016/j.ejmech.2014.07.054.
[19] S. Cascioferro, A. Attanzio, V. Di Sarno, S. Musella, L. Tesoriere, G. Cirrincione, P. Diana, B. Parrino, New 1,2,4-oxadiazole nortopsentin derivatives with cytotoxic activity, Mar. Drugs 17 (2019), https://doi.org/10.3390/md17010035.
[20] B. Parrino, A. Attanzio, V. Spanò, S. Cascioferro, A. Montalbano, P. Barraja, L. Tesoriere, P. Diana, G. Cirrincione, A. Carbone, Synthesis, antitumor activity and CDK1 inhibiton of new thiazole nortopsentin analogues, Eur. J. Med. Chem. 138 (2017) 371–383, https://doi.org/10.1016/j.ejmech.2017.06.052.
[21] V. Spanò, A. Attanzio, S. Cascioferro, A. Carbone, A. Montalbano, P. Barraja, L. Tesoriere, G. Cirrincione, P. Diana, B. Parrino, Synthesis and Antitumor Activity of New Thiazole Nortopsentin Analogs, Mar. Drugs vol. 14 (2016), https://doi.org/10.3390/md14120226.
[22] B. Parrino, A. Carbone, G. Di Vita, C. Ciancimino, A. Attanzio, V. Spanò, A. Montalbano, P. Barraja, L. Tesoriere, M.A. Livrea, P. Diana, G. Cirrincione, 3-[4-(1H-Indol-3-yl)-1,3-thiazol-2-yl]-1H-pyrrolo[2,3-b]pyridines, nortopsentin analogues with antiproliferative activity, Mar. Drugs 13 (2015) 1901–1924, https://doi.org/10.3390/md13041901.
[23] A. Carbone, B. Parrino, G. Di Vita, A. Attanzio, V. Spanò, A. Montalbano, P. Barraja, L. Tesoriere, M.A. Livrea, P. Diana, G. Cirrincione, Synthesis and antiproliferative activity of thiazolyl-bis-pyrrolo[2,3-*b*]pyridines and indolyl-thiazolyl-pyrrolo[2,3-c]pyridines, nortopsentin analogues, Mar. Drugs 13 (2015) 460–492, https://doi.org/10.3390/md13010460.
[24] P. Diana, A. Stagno, P. Barraja, A. Montalbano, A. Carbone, B. Parrino, G. Cirrincione, Synthesis of the new ring system pyrrolizino[2,3-b]indol-4(5H)-one, Tetrahedron 67 (2011) 3374–3379, https://doi.org/10.1016/j.tet.2011.03.060.
[25] P. Barraja, L. Caracausi, P. Diana, V. Spanò, A. Montalbano, A. Carbone, B. Parrino, G. Cirrincione, Synthesis and antiproliferative activity of the ring system [1,2]oxazolo[4,5-g]indole, ChemMedChem 7 (2012) 1901–1904, https://doi.org/10.1002/cmdc.201200296.
[26] P. Diana, A. Stagno, P. Barraja, A. Carbone, B. Parrino, F. Dall'Acqua, D. Vedaldi, A. Salvador, P. Brun, I. Castagliuolo, O.G. Issinger, G. Cirrincione, Synthesis of triazenoazaindoles: a new class of triazenes with antitumor activity, ChemMedChem 6 (2011) 1291–1299, https://doi.org/10.1002/cmdc.201100027.
[27] A. Carbone, M. Pennati, B. Parrino, A. Lopergolo, P. Barraja, A. Montalbano, V. Spanò, S. Sbarra, V. Doldi, M. De Cesare, G. Cirrincione, P. Diana, N. Zaffaroni, Novel 1H-pyrrolo[2,3-b]pyridine derivative nortopsentin analogues: synthesis and antitumor activity in peritoneal mesothelioma experimental models, J. Med. Chem. 56 (2013) 7060–7072, https://doi.org/10.1021/jm400842x.
[28] G. Li Petri, S. Cascioferro, B. El Hassouni, D. Carbone, B. Parrino, G. Cirrincione, G.J. Peters, P. Diana, E. Giovannetti, Biological evaluation of the antiproliferative and anti-migratory activity of a series of 3-(6-Phenylimidazo [2,1-b][1,3,4]thiadiazol-2-yl)-1H-indole derivatives against pancreatic cancer cells, Anticancer Res. 39 (2019) 3615–3620, https://doi.org/10.21873/anticanres.13509.
[29] B. Parrino, A. Carbone, C. Ciancimino, V. Spanò, A. Montalbano, P. Barraja, G. Cirrincione, P. Diana, C. Sissi, M. Palumbo, O. Pinato, M. Pennati, G. Beretta, M. Folini, P. Matyus, B. Balogh, N. Zaffaroni, Water-soluble isoindolo[2,1-a] quinoxalin-6-imines: in vitro antiproliferative activity and molecular mechanism(s) of action, Eur. J. Med. Chem. 94 (2015) 149–162, https://doi.org/10.1016/j.ejmech.2015.03.005.
[30] B. Parrino, S. Ullo, A. Attanzio, S. Cascioferro, V. Spanò, A. Carbone, A. Montalbano, P. Barraja, G. Cirrincione, L. Tesoriere, P. Diana, Synthesis of 5H-pyrido[3,2-b]pyrrolizin-5-one tripentone analogs with antitumor activity, Eur. J. Med. Chem. 158 (2018) 236–246, https://doi.org/10.1016/j.ejmech.2018.09.017.
[31] B. Parrino, S. Ullo, A. Attanzio, V. Spanò, S. Cascioferro, A. Montalbano, P. Barraja, L. Tesoriere, G. Cirrincione, P. Diana, New tripentone analogs with antiproliferative activity, Molecules 22 (2017), https://doi.org/10.3390/molecules22112005.
[32] B. Parrino, A. Carbone, V. Spanò, A. Montalbano, D. Giallombardo, P. Barraja, A. Attanzio, L. Tesoriere, C. Sissi, M. Palumbo, G. Cirrincione, P. Diana, Azaisoindolo and isoindolo-azaquinoxaline derivatives with antiproliferative activity, Eur. J. Med. Chem. 94 (2015) 367–377, https://doi.org/10.1016/j.ejmech.2015.03.009.
[33] B. Parrino, A. Carbone, M. Muscarella, V. Spanò, A. Montalbano, P. Barraja, A. Salvador, D. Vedaldi, G. Cirrincione, P. Diana, 11H-Pyrido[3′,2′:4,5]pyrrolo [3,2-c]cinnoline and pyrido[3′,2′:4,5]pyrrolo[1,2-c][1,2,3]benzotriazine: two new ring systems with antitumor activity, J. Med. Chem. 57 (2014) 9495–9511, https://doi.org/10.1021/jm501244f.
[34] B. Parrino, C. Ciancimino, A. Carbone, V. Spano, A. Montalbano, P. Barraja, G. Cirrincione, P. Diana, Synthesis of isoindolo[1,4]benzoxazinone and isoindolo[1,5]benzoxazepine: two new ring systems of pharmaceutical interest, Tetrahedron 71 (2015) 7332–7338, https://doi.org/10.1016/j.tet.2015.04.083.
[35] A. Montalbano, B. Parrino, P. Diana, P. Barraja, A. Carbone, V. Spanò, G. Cirrincione, Synthesis of the new oligopeptide pyrrole derivative isonetropsin and its one pyrrole unit analogue, Tetrahedron 69 (2013) 2550–2554, https://doi.org/10.1016/j.tet.2013.01.076.
[36] E. Giovannetti, C.L. van der Borden, A.E. Frampton, A. Ali, O. Firuzi, G.J. Peters, Never let it go: stopping key mechanisms underlying metastasis to fight pancreatic cancer, Semin. Canc. Biol. 44 (2017) 43–59, https://doi.org/10.1016/j.semcancer.2017.04.006.
[37] C. Nevala-Plagemann, M. Hidalgo, I. Garrido-Laguna, From state-of-the-art treatments to novel therapies for advanced-stage pancreatic cancer, Nat. Rev. Clin. Oncol. 17 (2020) 108–123, https://doi.org/10.1038/s41571-019-0281-6.
[38] E. Razi, M. Radak, M. Mahjoubin-Tehran, S. Talebi, A. Shafiee, S. Hajighadimi, S. Moradizarmehri, H. Sharifi, N. Mousavi, M. Sarvizadeh, M. Nejati, M. Taghizadeh, F. Ghasemi, Cancer stem cells as therapeutic targets of pancreatic cancer, Fundam, Clin. Pharmacol. (2019), https://doi.org/10.1111/fcp.12521. In press.
[39] H.R. Mirzaei, A. Sahebkar, R. Salehi, J.S. Nahand, E. Karimi, M.R. Jaafari, H. Mirzaei, Boron neutron capture therapy: moving toward targeted cancer therapy, J. Canc. Res. Therapeut. 12 (2016) 520–525, https://doi.org/10.4103/0973-1482.176167.
[40] H.R. Mirzaei, H. Mirzaei, S.Y. Lee, J. Hadjati, B.G. Till, Prospects for chimeric antigen receptor (CAR) γδ T cells: a potential game changer for adoptive T cell cancer immunotherapy, Canc. Lett. 380 (2016) 413–423, https://doi.org/10.1016/j.canlet.2016.07.001.
[41] M. Amrutkar, I.P. Gladhaug, Pancreatic cancer chemoresistance to gemcitabine, Cancers 9 (2017) 157, https://doi.org/10.3390/cancers9110157.
[42] R. Sciarrillo, A. Wojtuszkiewicz, I.E. Kooi, V.E. Gómez, U. Boggi, G. Jansen, G.-J. Kaspers, J. Cloos, E. Giovannetti, Using RNA-sequencing to detect novel splice variants related to drug resistance in in vitro cancer models, JoVE 118 (2016) e54714, https://doi.org/10.3791/54714.
[43] T.Y.S. Le Large, B. El Hassouni, N. Funel, B. Kok, S.R. Piersma, T.V. Pham, K.P. Olive, G. Kazemier, H.W.M. van Laarhoven, C.R. Jimenez, M.F. Bijlsma, E. Giovannetti, Proteomic analysis of gemcitabine-resistant pancreatic cancer cells reveals that microtubule-associated protein 2 upregulation associates with taxane treatment, Ther Adv Med Oncol 11 (2019), https://doi.org/10.1177/1758835919841233, 1758835919841233.
[44] A. Avan, V. Caretti, N. Funel, E. Galvani, M. Maftouh, R.J. Honeywell, T. Lagerweij, O. Van Tellingen, D. Campani, D. Fuchs, H.M. Verheul, G.-J. Schuurhuis, U. Boggi, G.J. Peters, T. Würdinger, E. Giovannetti, Crizotinib inhibits metabolic inactivation of gemcitabine in c-Met-driven pancreatic carcinoma, Canc. Res. 73 (2013) 6745–6756, https://doi.org/10.1158/0008-5472.CAN-13-0837.
[45] S. Sant, P.A. Johnston, The production of 3D tumor spheroids for cancer drug discovery, Drug Discov. Today Technol. 23 (2017) 27–36, https://doi.org/10.1016/j.ddtec.2017.03.002.
[46] O. Firuzi, P.P. Che, B. El Hassouni, M. Buijs, S. Coppola, M. Löhr, N. Funel, R. Heuchel, I. Carnevale, T. Schmidt, G. Mantini, A. Avan, L. Saso, G.J. Peters, E. Giovannetti, Role of c-MET inhibitors in overcoming drug resistance in spheroid models of primary human pancreatic cancer and stellate cells, Cancers 11 (2019), https://doi.org/10.3390/cancers11050638.
[47] J.P. Thiery, H. Acloque, R.Y.J. Huang, M.A. Nieto, Epithelial-mesenchymal transitions in development and disease, Cell 139 (2009) 871–890, https://doi.org/10.1016/j.cell.2009.11.007.
[48] A. Puisieux, T. Brabletz, J. Caramel, Oncogenic roles of EMT-inducing transcription factors, Nat. Cell Biol. 16 (2014) 488–494, https://doi.org/10.1038/ncb2976.
[49] S. Valastyan, R.A. Weinberg, Tumor metastasis: molecular insights and evolving paradigms, Cell 147 (2011) 275–292, https://doi.org/10.1016/j.cell.2011.09.024.
[50] E. Batlle, E. Sancho, C. Francí, D. Domínguez, M. Monfar, J. Baulida, A. García de Herreros, The transcription factor Snail is a repressor of *E-cadherin* gene expression in epithelial tumour cells, Nat. Cell Biol. 2 (2000) 84–89, https://doi.org/10.1038/35000034.
[51] A. Cano, M.A. Pérez-Moreno, I. Rodrigo, A. Locascio, M.J. Blanco, M.G. del Barrio, F. Portillo, M.A. Nieto, The transcription factor Snail controls epithelial–mesenchymal transitions by repressing E-cadherin expression, Nat. Cell Biol. 2 (2000) 76–83, https://doi.org/10.1038/35000025.
[52] K.M. Hajra, D.Y.-S. Chen, E.R. Fearon, The SLUG zinc-finger protein represses E-cadherin in breast cancer, Canc. Res. 62 (2002) 1613–1618.
[53] S. Nakajima, R. Doi, E. Toyoda, S. Tsuji, M. Wada, M. Koizumi, S.S. Tulachan, D. Ito, K. Kami, T. Mori, Y. Kawaguchi, K. Fujimoto, R. Hosotani, M. Imamura, N-cadherin expression and epithelial-mesenchymal transition in pancreatic carcinoma |Clinical cancer research, Clin. Canc. Res. (2004) 4125–4133.
[54] S. Wang, S. Huang, Y.L. Sun, Epithelial-mesenchymal transition in pancreatic cancer: a review, BioMed Res. Int. (2017) 2646148, https://doi.org/10.1155/

2017/2646148.
[55] L.L. Meijer, I. Garajová, C. Caparello, T.Y.S. Le Large, A.E. Frampton, E. Vasile, N. Funel, G. Kazemier, E. Giovannetti, Plasma miR-181a-5p downregulation predicts response and improved survival after FOLFIRINOX in pancreatic ductal adenocarcinoma, Ann. Surg. (2018), https://doi.org/10.1097/SLA.0000000000003084. In press.
[56] J.E. Hall, W. Fu, M.D. Schaller, Chapter five - focal adhesion kinase: exploring FAK structure to gain insight into function, Inter. Rev. Cell Mol. Bio. 288 (2011) 185–225, https://doi.org/10.1016/B978-0-12-386041-5.00005-4.
[57] J. Zhou, Q. Yi, L. Tang, The roles of nuclear focal adhesion kinase (FAK) on Cancer: a focused review, J. Exp. Clin. Canc. Res. 38 (2019) 250, https://doi.org/10.1186/s13046-019-1265-1.
[58] R. Kanteti, S.K. Batra, F.E. Lennon, R. Salgia, FAK and paxillin, two potential targets in pancreatic cancer, Oncotarget 7 (2016) 31586–31601, https://doi.org/10.18632/oncotarget.8040.
[59] J.-N. Ho, W. Jun, R. Choue, J. Lee, I3C and ICZ inhibit migration by suppressing the EMT process and FAK expression in breast cancer cells, Mol. Med. Rep. 7 (2013) 384–388, https://doi.org/10.3892/mmr.2012.1198.
[60] A. Carbone, B. Parrino, M.G. Cusimano, V. Spanò, A. Montalbano, P. Barraja, D. Schillaci, G. Cirrincione, P. Diana, S. Cascioferro, New thiazole nortopsentin analogues inhibit bacterial biofilm formation, Mar. Drugs 16 (2018) 274, https://doi.org/10.3390/md16080274.
[61] E. Giovannetti, N. Funel, G.J. Peters, M.D. Chiaro, L.A. Erozenci, E. Vasile, L.G. Leon, L.E. Pollina, A. Groen, A. Falcone, R. Danesi, D. Campani, H.M. Verheul, U. Boggi, MicroRNA-21 in pancreatic cancer: correlation with clinical outcome and pharmacologic aspects underlying its role in the modulation of gemcitabine activity, Canc. Res. 70 (2010) 4528–4538, https://doi.org/10.1158/0008-5472.CAN-09-4467.
[62] D. Massihnia, A. Avan, N. Funel, M. Maftouh, A. van Krieken, C. Granchi, R. Raktoe, U. Boggi, B. Aicher, F. Minutolo, A. Russo, L.G. Leon, G.J. Peters, E. Giovannetti, Phospho-Akt overexpression is prognostic and can be used to tailor the synergistic interaction of Akt inhibitors with gemcitabine in pancreatic cancer, J. Hematol. Oncol. 10 (2017) 9, https://doi.org/10.1186/s13045-016-0371-1.
[63] R. Sciarrillo, A. Wojtuszkiewicz, B. El Hassouni, N. Funel, P. Gandellini, T. Lagerweij, S. Buonamici, M. Blijlevens, E.A. Zeeuw van der Laan, N. Zaffaroni, M. Deraco, S. Kusamura, T. Würdinger, G.J. Peters, C.F.M. Molthoff, G. Jansen, G.J.L. Kaspers, J. Cloos, E. Giovannetti, Splicing modulation as novel therapeutic strategy against diffuse malignant peritoneal mesothelioma, EBioMedicine 39 (2019) 215–225, https://doi.org/10.1016/j.ebiom.2018.12.025.
[64] I. Garajová, T.Y.S. Le Large, E. Giovannetti, G. Kazemier, G. Biasco, G.J. Peters, The role of MicroRNAs in resistance to current pancreatic cancer treatment: translational studies and basic protocols for extraction and PCR analysis, Methods Mol. Biol. 1395 (2016) 163–187, https://doi.org/10.1007/978-1-4939-3347-1_10.
[65] S. La Monica, C. Caffarra, F. Saccani, E. Galvani, M. Galetti, C. Fumarola, M. Bonelli, A. Cavazzoni, D. Cretella, R. Sirangelo, R. Gatti, M. Tiseo, A. Ardizzoni, E. Giovannetti, P.G. Petronini, R.R. Alfieri, Gefitinib inhibits invasive phenotype and epithelial-mesenchymal transition in drug-resistant NSCLC cells with MET amplification, PloS One 8 (2013), e78656, https://doi.org/10.1371/journal.pone.0078656.
[66] E. Giovannetti, M. Labots, H. Dekker, E. Galvani, J.S.W. Lind, R. Sciarrillo, R. Honeywell, E.F. Smit, H.M. Verheul, G.J. Peters, Molecular mechanisms and modulation of key pathways underlying the synergistic interaction of sorafenib with erlotinib in non-small-cell-lung cancer (NSCLC) cells, Curr, Pharm. Des. 19 (2013) 927–939.
[67] N.V.D. Steen, L. Potze, E. Giovannetti, A. Cavazzoni, R. Ruijtenbeek, C. Rolfo, P. Pauwels, G.J. Peters, Molecular mechanism underlying the pharmacological interactions of the protein kinase C-β inhibitor enzastaurin and erlotinib in non-small cell lung cancer cells, Am. J. Cancer Res. 7 (2017) 816–830.